2008

Methane And Dimethyl Ether Oxidation At Elevated Temperatures And Pressure

Christopher Zinner
University of Central Florida

METHANE AND DIMETHYL ETHER OXIDATION AT ELEVATED TEMPERATURES AND PRESSURE

by

CHRISTOPHER MICHAEL ZINNER
B.S. University of Central Florida, 2006

A thesis submitted in partial fulfillment of the requirements
for the degree of Masters of Science in Mechanical Engineering
in the Department of Mechanical, Materials, and Aerospace Engineering
in the College of Engineering and Computer Science
at the University of Central Florida
Orlando, Florida

Spring Term
2008

ABSTRACT

Autoignition and oxidation of two Methane (CH_4) and Dimethyl Ether (CH_3OCH_3 or DME) mixtures in air were studied in shock tubes over a wide range of equivalence ratios at elevated temperatures and pressures. These experiments were conducted in the reflected shock region with pressures ranging from 0.8 to 35.7 atmospheres, temperatures ranging from 913 to 1650 K, and equivalence ratios of 2.0, 1.0, 0.5, and 0.3. Ignition delay times were obtained from shock-tube endwall pressure traces for fuel mixtures of CH_4/CH_3OCH_3 in ratios of 80/20 percent volume and 60/40 percent volume, respectively. Close examination of the data revealed that energy release from the mixture is occurring in the time between the arrival of the incident shock wave and the ignition event. An adjustment scheme for temperature and pressure was devised to account for this energy release and its effect on the ignition of the mixture. Two separate ignition delay correlations were developed for these pressure- and temperature-adjusted data. These correlations estimate ignition delay from known temperature, pressure, and species mole fractions of methane, dimethyl ether, and air ($0.21\ O_2 + 0.79\ N_2$). The first correlation was developed for ignition delay occurring at temperatures greater than or equal to1175 K and pressures ranging from 0.8 to 35.3 atm. The second correlation was developed for ignition delay occurring at temperatures less than or equal to1175 K and pressures ranging from 18.5 to 40.0 atm. Overall good agreement was found to exist between the two correlations and the data of these experiments. Findings of these experiments also include that with pressures at or below ten atm, increased concentrations of dimethyl ether will consistently produce faster ignition times. At pressures greater than ten atmospheres it is possible for fuel rich mixtures with lower concentrations of dimethyl ether to give the fastest ignition times.

This work represents the most thorough shock tube investigation for oxidation of methane with high concentration levels of dimethyl ether at gas turbine engine relevant temperatures and pressures. The findings of this study should serve as a validation for detailed chemical kinetics mechanisms.

To my parents and my brother.

TABLE OF CONTENTS

LIST OF FIGURES viii

LIST OF TABLES xii

LIST OF SYMBOLS AND ABREVIATIONS xiii

CHAPTER 1: INTRODUCTION 1

CHAPTER 2: BACKGROUND LITERATURE REVIEW 6

2.1 Combustion and gas turbines 6

2.2 Methane oxidation 7

2.3 Dimethyl ether oxidation 9

CHAPTER 3: METHODOLOGY 22

3.1 Apparatus and procedure 22

3.2 Mixtures 27

3.3 Ignition delay analysis 28

3.4 Pressure and temperature adjustments 30

3.5 Correlation development 33

CHAPTER 4: RESULTS 35

4.1 Adjustments 35

4.2 Data plots 38

4.3 Correlation 48

CHAPTER 5: CONCLUSIONS AND RECOMMENDATIONS 52

5.1 Conclusions 52

5.2 Recommendations 52

APPENDIX: TABULATED DATA 54

LIST OF REFERENCES 60

LIST OF FIGURES

Figure 1: Drawing of basic Premixing Circuit to Main Combustor section of gas turbine [8]. 3

Figure 2: Overall reaction scheme for dimethyl ether oxidation [10]. 10

Figure 3: Schematic representation of HO2 radical formation pathways in the Cl atom initiated oxidation of DME [29]..... 19

Figure 4: Schematic of the Aerospace Corporation's shock tube facility [37]. Only the lower shock tube was used in these experiments. 23

Figure 5: Schematic of the shock tube facility presented in Aul et al. [38]..... 24

Figure 6: Emission and pressure traces for Mix #8 at P = 7.9 atm and T = 1262 K..... 29

Figure 7: Explanation of pressure adjustments for a characteristic pressure trace. 30

Figure 8: Ignition delay and correlation data for mix #1. Low temperature correlation under-predicts at lower pressures. All others show good agreement. 38

Figure 9: Ignition delay and correlation data for mix #2. Low temperature correlation over predicts high pressure data. All others show good agreement. 39

Figure 10: Ignition delay and correlation data for mix #3. The low temperature correlation makes a slight over prediction of data at lower pressures. The low temperature correlation also over predicts the data at intermediate temperatures. 39

Figure 11: Ignition delay and correlation data for mix#4. The slope of the correlation curves appears to be shallower than the data. This would suggest that this lean data has higher activation energy than what is found in either the high and low temperature correlations. 40

Figure 12: Ignition delay and correlation data for mix#5. There is generally good agreement between correlation and data with high temperature correlation giving some over-prediction at higher pressures. Waviness in the correlation is likely due to the fluctuations in pressure between data points. 40

Figure 13: Ignition delay and correlation data for mix#6. Good agreement exists between high temperature correlation and two lower pressure data series, but the correlation tends to over-predict at higher pressures. The Lower temperature correlation does a fair job predicting ignition delay. 41

Figure 14: Ignition delay and correlation data for mix#7. The high temperature correlation tends to under predict the mid range and high pressure data, while the low temperature correlation appears to have an activation energy which is lower than that of the data..... 41

Figure 15: Ignition delay and correlation data for mix#8. The high temperature correlation appears to be in fair agreement with the data while the low temperature correlation seems to have an activation energy which is too low for this data..... 42

Figure 16: Comparison of equivalence ratios for ignition delay data of 80%CH_4 – 20%DME mixtures with similar adjusted temperatures and pressures. Data show similar ignition delay between 1370-1425 K. 44

Figure 17: Comparison of equivalence ratios for ignition delay data of 60%CH_4 – 40%DME mixtures with similar adjusted temperatures and pressures. Stoichiometric and rich data cross at approximately 1390 K; lean data merge at temperatures ranging from 1230-1350 K..... 44

Figure 18: Ignition delay data for 80%CH_4 – 20% DME mixtures with similar adjusted temperatures and pressures. The fuel rich mixture is the slowest to ignite while the others are similar for T > 1400 K. 45

Figure 19: Ignition delay data for 60%CH_4 – 40%DME mixtures with similar adjusted temperatures and pressures. The fuel rich mixture is the slowest of the four equivalence ratios at temperatures hotter than 1300 K, but becomes the fastest for temperatures less than 1275 K. 45

Figure 20: Comparison of fuel mixtures with ignition delay times for ϕ = 2.0, 0.5 mixtures with similar adjusted temperatures and pressures. The differences in mixtures are more pronounced at cooler temperatures. 46

Figure 21: Comparison of fuel mixtures with ignition delay times for ϕ = 1.0, 0.3 mixtures with similar adjusted temperatures and pressures. The ϕ = 1.0 mixture of the 80/20 mix has an ignition delay profile similar to that of the 60/40 ϕ = 0.3 mixture. 46

Figure 22: Comparison of mixtures for similar adjusted pressures and temperatures. With a few exceptions, the mixture having the greatest concentration of DME has the faster ignition times. 47

Figure 23: Comparison of mixtures of similar adjusted pressures and temperatures. In much the same way as Fig. 25, the mixture which contains the higher concentration produces the faster ignition time. 47

Figure 24: Parity plot for experimental results against the high temperature correlation. Ignition times in μs. 49

Figure 25: Parity plot for experimental results against the low temperature correlation. Ignition times in μs. 50

Figure 26: Comparison of data from both shock tube facilities. Pressure adjustments for ignition delay times from the high temperature correlation allow a better comparison of these two data series. 51

LIST OF TABLES

Table 1: Mixtures and targeted pressures of this work. Temperatures are dictated by the requirement that $\tau_{ign} > 50$ μs. 27

Table 2: Available diaphragms and the range of typical reflected shock pressures each can deliver. 35

Table 3: Average pressures obtained for each mixture. 36

Table 4: Sample results of pressure and temperature adjustments. Average change in temperature for all data is 13.9 K, and average change is pressure is 0.8 atm. 37

LIST OF SYMBOLS AND ABREVIATIONS

ϕ	Equivalence ratio
τ_1	First pressure rises due to chemical reaction as seen at the endwall
τ_{ign}	Ignition delay, evaluated at the endwall
atm	Pressure, atmospheres
BMEP	Break mean effective pressure
CH_4	Methane
CH_3OCH_3	Dimethyl ether, chemical formula
CO	Carbon monoxide
DME	Dimethyl ether, abbreviation
E_a	Activation energy
FTIR	Fourier transform infrared spectroscopy
LLNL	Lawrence Livermore National Laboratory
LPG	Liquefied petroleum gas
LPP	Lean premix prevaporize combustors
NOx	Oxides of nitrogen
P	Pressure
ppm	Parts per million
R_u	Universal gas constant
UNC	Unburned hydrocarbons
VPFR	Variable pressure flow reactor

CHAPTER 1: INTRODUCTION

The primary focus of this thesis is the oxidation of methane and dimethyl ether in shock tubes. This information is especially applicable to natural gas powered gas turbines, particularly those ground based, stationary units used in electrical power generation. The power generation industry has a long history of increasingly more stringent restrictions being placed upon emissions. This has been followed by continued progress towards lean-burning technologies because lean-burning systems offer the potential for greatest fuel efficiency while reducing the formation of undesirable combustion products such as Nitrogen Oxides and soot.

A good description of the design of modern gas turbines is present by Lefebvre [1]. Fundamentally, these systems rely on the burning of fossil fuels to release energy which is then converted into rotational mechanical work by turbine blades. For power generation, this rotational work is then used to spool electrical generators. Many gas turbines for power generation are derived from models designed for use with an aircraft platform. This allows for the cross compatibility of a great many engine parts, reducing the overall costs of production. In aircraft engine gas turbines, the fuel used is typically petroleum-based liquid hydrocarbons. The fuel is combined with compressed air in the combustor section through atomization by means of spray nozzles, aerodynamics, or often a combination of the two, and allowed to burn in a combination of diffusion and premixed flames. In power generation gas turbines, the modern approach to combustion is often different and more complex.

This difference is motivated by the desire to produce electrical power at a minimum operational cost while curtailing the undesirable residuals of combustion (soot, NOx, CO, etc.).

Because natural gas is an abundant, clean-burning, economical fuel source, the option to use this particular fuel is a compelling choice.

There is no rule which requires that a gas turbine powered by natural gas can not have a fuel delivery system similar to one that is used with liquid petroleum hydrocarbon fuels. Gaseous fuel could be directly injected into the combustors of the engine and with perhaps a few modest changes could operate in much the same manner as it would with the traditional liquid sprayed fuels. In fact, early usage of natural gas in gas turbines used the direct injection method. The problem with this scenario is that the full potential of the natural gas is not realized. Though there may be a cost benefit to using this particular fuel over its liquid counterpart, the maximum possible clean-burning potential of the natural gas has not been realized.

Diffusion flames typically burn at equivalence ratios close to unity. This creates "hot zones" in the combustion chamber where NOx formation is likely to occur. In order to mitigate this phenomenon, premixed flames are an attractive option and natural gas lends itself to this occasion.

To facilitate premixed flames, the aviation platform gas turbine must be extensively modified. Changes to the system include the routing of compressed air from the compressor section into a separate premixing circuit. Fuel is then combined with the compressed air, mixed to the desired equivalence ratio, and throttled into the combustors where it is burned. A basic schematic of this process is shown in Fig. 1.

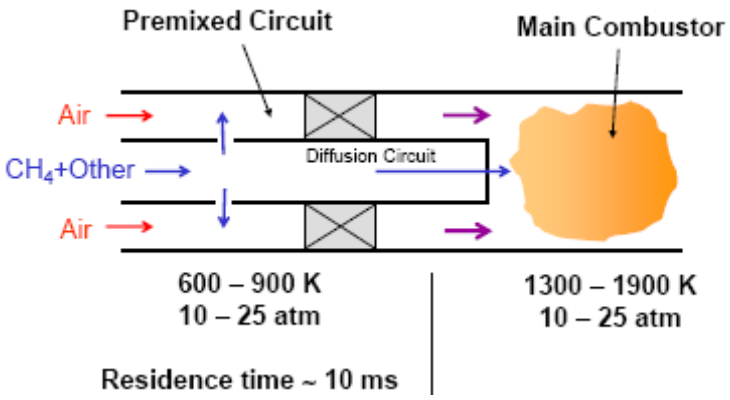

Figure 1: Drawing of basic Premixing Circuit to Main Combustor section of gas turbine [8].

When perfected, the premixing circuit method of fuel induction will allow for a burner system with a minimal level of undesirable combustion products; however, the attainment of such a state is not merely so trivial. Complications associated with combustion can occur if the design of the premixing circuit is not adequate. These possible complications include: autoignition within the premixing circuit, flashback, blowoff, and general flame instability.

Autoignition involves the self igniting of a fuel with an oxidizer when that mixture crosses a requisite energy barrier necessary to sustain oxidation reaction. This energy barrier can vary greatly, depending on the particular fuel and oxidizer, and the relative abundance of each.

Flashback involves the back flow of the combustion reaction from its intended location within the combustor, back into the premixing circuit. This may result in damage to the premixing circuit.

Blowoff occurs when the flow rate through the combustor exceeds the flame speed of the fuel/air mix, resulting in combustion occurring downstream of the combustor. Blowoff can also occur when the mixture strength is too weak; having an equivalence ratio which is too close to

either of the extremeum making it too lean or too rich to sustain combustion within the desired combustion zone of the gas turbine.

A parallel can be drawn between each of these modes of failure – they each can happen if designers of the gas turbine systems do not structure their design around the chemical kinetics of the fuel their system will employ. For this reason, it is essential to obtain a detailed understanding of the chemical kinetics of fuels used in gas turbines. This information provides the engine designer knowledge for developing designs which are not only robust, but capable of delivering the required performance with regards to emission control.

Methane (CH_4) oxidation is of interest because it constitutes the bulk (upwards of 90% by volume) of what is commonly called Natural Gas. Methane is the simplest alkane and its oxidation characteristics are handily adjusted by the addition of trace amounts of other fuels [3]. Methane itself is one of the most extensively studied fuels [4,5]; however, small amounts of higher order hydrocarbons impurities are commonly found in natural gas. These impurities can have significant effects on methane oxidation, especially near the lean limit of combustion. It is desirable to operate the gas turbine in close proximity to this lean limit of combustion from an emissions perspective. The effects of these impurities on lean premixed natural gas flames can result in engine problems such as those previously mentioned. This fact has prompted many authors to study the effects of higher order hydrocarbons on methane oxidation [6,39], and has driven others to study combustor design for the purpose of developing combustors which can maintain optimal performance despite a wide range of natural gas compositions [2].

In this study, dimethyl ether (CH_3OCH_3 or DME for short) is the fuel additive of interest. DME is the simplest of all ethers. It has the same empirical formula as ethanol (C_2H_6O). In the 1990s DME became popular with engine researchers, having been discovered as a promising

alternative fuel for diesel engines. DME, with its cetane numbers ranging from 55-60, would promote ignition in diesel fuels. Pure DME flames have been found to be almost completely sootless. DME could be blended with diesel fuel up to a solubility limit of approximately 10% by volume. Doing this showed to benefit emissions with an overall reduction in soot.

Having demonstrated such promise with diesel engines, attention has gradually migrated towards the use of DME with gas turbines in combination with their most common fuels. This leads us to the present study of methane and DME oxidation with methane being the base fuel due to its prominence in natural gas. Details on the background literature for both methane and dimethyl ether are given in Chapter 2.

In this work, the chosen methodology for the study of methane/DME oxidation is the shock tube. A good description of what a shock tube is and how it is used is presented in Gaydon and Hurle [33]. The shock tube is a device with which normal shock waves are used to study a wide range of subjects. Specific to the needs of this study, shock waves are used to compress and thereby heat a mixture of fuel and air nearly instantaneously with minimal boundary layer effects. This ability allows for the observation of pure chemical kinetic phenomena which is highly useful to the study of combustion.

Following this introduction, a review of the background literature for these two fuels is presented in Chapter 2. Details on the experimental apparatus and its implementation along with a description of the objectives of this study are given in Chapter 3. In Chapter 4, the findings of these experiments are presented along with a discussion of their analysis. Finally, conclusions are drawn about these findings and offered in Chapter 5 along with recommendations for future experiments.

CHAPTER 2: BACKGROUND LITERATURE REVIEW

2.1 Combustion and gas turbines

The approach to gas turbine combustor design during the twentieth century is well documented in the aptly named book "Gas Turbine Combustion" 2nd Edition, by A. H. Lefebvre [1]. In this book the author takes the reader through the design points and motivation of combustor design from the earliest gas turbines, to modern aviation and industrial combustors. Of particular interest to the work of this thesis is the development of combustors for use with natural gas powered gas turbines for industrial applications. The author is quick to point out that the requirements of low emission are in conflict with performance and that modifications to combustors that favor the reduction of soot and oxides of nitrogen (NOx) almost invariably result in the increased emission of other undesirables such as unburned hydrocarbons (UNC) and carbon monoxide (CO). The reverse of this is often true as well with reductions in UNC and CO giving way to higher levels of soot and NOx [1].

Lefebvre details several avenues for combating these pollutants simultaneously. One method involves the use of variable geometry to regulate the amount of air entering the primary combustion zone. Another widely used practice involves the "staging" of combustion, where combustion takes place in two or more zones and each zone is optimized for a specific aspect of combustion. For ultra low NOx combustion, the preferred method is to use lean premixed prevaporized (LPP) combustors. Examples of aeroderivative gas turbine engines which use LPP technology are the GE LM6000 and the RR211 DLE.

Flores et al. [2] evaluated the effects of natural gas fuel composition on the performance of a model gas turbine combustor. Their approach was to vary the amounts of methane, ethane,

and propane, and analyze what effects this has on the operation of the model combustor. The findings of this work include that fuel composition plays a significant role in NOx emission and that higher order hydrocarbons generate more NOx for a given firing temperature, independent of mixing. They attributed this to nonthermal NOx formation pathways which depend upon fuel composition. They also found that it would be possible to maintain a level of acceptable performance while compensating for NOx by implementing an adaptive fuel injection strategy [2].

2.2 Methane oxidation

The literature for methane oxidation is extensive, having been studied by a great many authors, over a very wide range of pressures, temperatures, equivalence ratios, and with a great diversity of experimental methodologies. A complete review of the literature concerning methane oxidation is beyond the scope of this thesis; instead, what is offered is a review of methane oxidation such that would be sufficient enough to understand the essential progress made towards natural gas research.

In 1994, a good, comprehensive summary of the study of methane oxidation was presented in a paper by Spadaccini and Colket [3]. Besides summarizing the literature for methane, they also undertook experiments to determine ignition delay times for mixtures of methane with ethane, propane, or butane. Ignition delay times were found in shock tubes for mixtures with equivalence ratios of 0.45-1.25, temperatures of 1300-2000 K, pressures of 3-15 atm, and from these data an empirical expression was developed for the ignition delay time as a function of activation energy, temperature, and species concentration.

In 1999, Petersen at al. [4] conducted an analytical study to supplement the then recent high-pressure shock tube work for CH_4/O_2. The work included pressures of 40-260 atm, temperatures of 1040-1500 K, and equivalence ratios as high as 6 with a focus on low dilution. This work served to bridge the gap in kinetics modeling between low- to intermediate-temperature and high-pressure kinetic models for CH_4.

In 2003, Huang et al. [5] studied methane oxidation in air with shock tubes at temperatures of 1000-1350 K, pressures of 16-40 atm, and equivalence ratios of 0.7-1.3. The motivation behind this work was to understand oxidation at internal combustion engine conditions. The results of their study were used to update the modeling of Petersen et al. [4].

In a work awaiting publication by Bourque et al. [6], the most comprehensive set of experimental ignition and laminar flame speed data available in the open literature for $CH_4/C_2H_6/C_3H_8/C_4H_{10}/C_5H_{12}$ fuel blends is presented. Experiments and modeling work were conducted for ignition delay and flame speed of methane mixtures containing significant levels of the heavier hydrocarbons ethane, propane, n-butane, and n-pentane. Shock-tube and rapid compression machine experiments were conducted for temperatures from 740-1660 K, pressures up to 36 atm, and equivalence ratios from 0.3-2.0. Flame speed measurements were made for pressures of up to 4 atm.

The motivation for much of the work mentioned is a greater understanding of the potential of natural gas. Methane is studied because it is the primary constituent of natural gas, and the presence of higher order hydrocarbons significantly affects the oxidation characteristics of methane-based fuels. In the next section of this chapter, the sequence of pertinent literature concerning dimethyl ether oxidation, pyrolysis, and oxidation with methane is presented.

2.3 Dimethyl ether oxidation

When many authors begin their literature reviews of dimethyl ether, they typically begin with the 1996 work of Pfahl and co-workers [7]. Their study contains the first shock-tube oxidation data for homogeneous DME/air mixtures. The study includes temperatures of approximately 660-1280 K, two pressure groupings of 40±2 and 13±1.5 bar, an equivalence ratio of 1.0, and test times approaching 10 ms. The extended test times were accomplished through means of a tailored interface (more information on the use of tailoring in shock tubes can be found in Amadio [33]). The larger objective of their study was to investigate the oxidation characteristics of diesel engine relevant hydrocarbon fuels under engine conditions. They tested three fuels: α-methylnaphthalene, n-decane, and DME. Within the temperature ranges of their experiments, it was found that DME had the fastest ignition delay of all fuels tested. DME was also found to exhibit negative temperature coefficient regions which exist between approximately 770-910 K at 13 bar. These shift towards hotter temperatures at 40 bar to approximately 820-970 K. DME also exhibits a pronounced two-step autoignition with the first-step occurring at temperatures below 800 K for a pressure of 13 bar and blow 840 K at 40 bar. The researchers also noted that at temperatures below 720 K, pressure plays a less significant role in ignition delay than it does for higher temperatures, where higher pressure was found to consistently give shorter ignition times.

Also in 1996 at the same conference as the above paper, Dagaut et al. [9] presented DME oxidation experiments in a jet-stirred reactor for pressures of 1 and 10 atm, equivalence ratios of 0.2 to 2.5, and temperatures of 800-1300 K. This study involved the gathering of concentration profiles of reactants, intermediates, and products essential to the oxidation of DME.

In 1997, Curran et al. [10] used the work of Pfahl and co-workers [7] and Dagaut et al. [9] as benchmarks for a chemical kinetics mechanism with 78 chemical species and 336 chemical reactions. Overall good agreement was found to exist between the model and experimental data, with the model showing the capability of accurately predicting both first stage "cool flame" ignition times and second stage total ignition times as seen in the work by Pfahl and co-workers [7]. The overall reaction scheme for DME oxidation as determined by Curran et al. is given in Fig. 2.

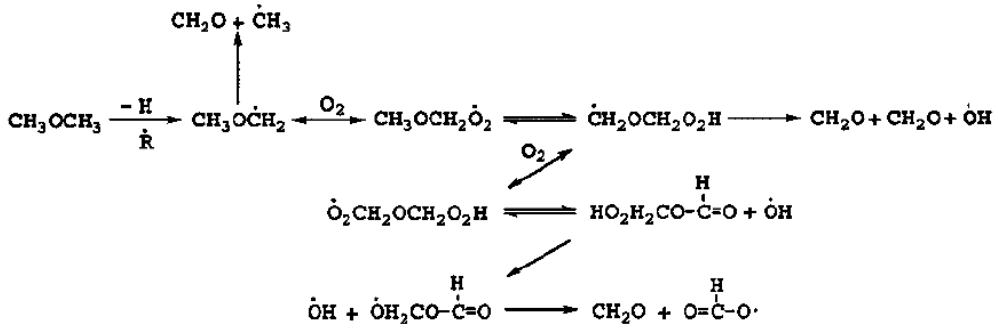

Figure 2: Overall reaction scheme for dimethyl ether oxidation [10].

In 1998, Amano and Dryer [11] conducted variable-pressure flow reactor experiments for methane oxidation with the addition of small amounts of DME, NOx, and ethane. Temperatures and pressures of these experiments were between 10-18 atm and 800-1060 K for similarity to conditions found in a spark- or compression-ignition engines. Equivalence ratios were varied from 0.5-2.0. The results of this study included the finding that a 1% DME addition to methane was as effective at promoting ignition as a 3% ethane addition to methane. NOx addition to methane was found to be the most effective at promoting ignition, even with additions only at a ppm level. Their work also included modeling. Ultimately, they decided to add a $CH_3 + NO_2 = CH_3 + NO_2$ reaction to GRI-Mech v2.11 [12] to capture the ignition phenomenon regarding NOx addition to methane oxidation.

In that same year, Dagaut et al. [13] presented work on DME oxidation from a jet stirred reactor at 10 atm, $0.2 \leq \phi \leq 1.0$, and 500-1100 K. Of particular interest to the researchers was the "cool flame" phenomenon, and at the listed temperatures and pressure they sampled reactants, intermediates, and products of oxidation within these "cool flames". The researchers also performed shock-tube experiments for the ignition delay times of DME/O_2/Ar mixtures at 3.5 atm for equivalence ratios of $0.5 \leq \phi \leq 2.0$. Along with the experimental work, modeling was performed for a detailed chemical kinetics mechanism with 331 mostly reversible reactions and 55 chemical species. This model was used to describe both the low and high-temperature oxidation of DME from previous experimental work. They included jet stirred reactor measurements at temperatures ranging between 550-1275 K and pressures between 1-10 atm, and shock-tube measurements for temperatures of 650-1600 K and pressures between 3.5-40 bar. The researchers found their model to be in general good agreement with the data.

One final DME study from 1998 by Frye et al. [14] measured the CO and NO emissions from DME, propane, and n-butane laminar premixed flames over a broad range of stoichiometries ($0.5 \leq \phi \leq 3.2$). The results of their experiments showed that DME emissions have lower CO content than do propane and n-butane over the range of equivalence ratios studied while NO production from DME was generally less or similar to propane and n-butane.

In 1999, the authors Fischer, Curran, and Dryer put forth a two-part series of papers regarding their combined modeling work on DME. The first paper, Fischer et al. [15], contained new flow reactor data for DME oxidation under highly dilute conditions and pyrolysis of DME. The pyrolysis studies were conducted in a variable-pressure flow reactor at 2.5 atm and 1118 K. Oxidation, trace oxygen assisted pyrolysis, and pyrolysis experiments were conducted in an atmospheric-pressure flow reactor at approximately 1085 K. In the oxidation experiments, the

equivalence ratio was varied such that $0.32 \leq \phi \leq 3.4$. These experiments provided validation data for the concentration of key chemical species at various times during the process of pyrolysis/combustion. Results of this work were a model which could accurately predict the ignition delay times of previous shock tube studies as well as the time history of most chemical species. The main discrepancy that existed between the model and experimental data concerned the chemical species profiles of methane at fuel-lean conditions. The authors were unsure as to the reason for this, because their model was able to fully explain product formation.

In the companion paper, Curran et al. [16], DME oxidation was studied in a variable-pressure flow reactor over an initial reactor temperature range of 550-850 K, pressure range of 12-18 atm, and equivalence ratios of $0.7 \leq \phi \leq 4.2$ with nitrogen dilution constituting 98.5% volume of the resultant mixture. The main finding of the experiments was that formic acid (CH_2O_2 or HCOOH) is a major intermediate chemical species in low-temperature DME oxidation. This information was used to update the modeling work of Curran et al. [10] to included chemistry leading to the formation of formic acid as well as chemistry for its oxidation. As a matter of protocol, the model of this work was also checked against the experimental findings of Pfahl and co-workers [7] and Dagaut et al. [9] and found to be in good agreement.

In 2000, Kaiser et al. [17] presented a study of atmospheric, premixed DME-air flames in a flat flame burner at equivalence ratios of $\phi = 0.67$ and $\phi = 1.49$. Temperature and chemical species profiles for CH_4, C_2H_2, C_2H_4, C_2H_6, C_3H_8, DME, CO, CO_2, O_2, CH_2O, and CH_2O_2 were monitored through the methods of gas chromatography and Fourier transform infrared spectroscopy (FTIR) with respect to the sampling probe's position within the reaction relative to the injector plate. Chemical species and additional temperature profiles were measured for premixed methane-air flames at equivalence ratios of $\phi = 0.74$ and $\phi = 1.47$ in order to provide a

reference for data analysis. The analysis found that mole fractions of C_2 product species were similar in DME and methane flames for similar equivalence ratios, but the mole fractions of CH_2O were found to be 5-10 times larger in the DME flames. This particular finding suggests that the dissociation of CH_3OCH_2 (methoxymethyl radicals) is predominantly occurring through the reaction $CH_3OCH_2 = CH_3 + CH_2O$ which is playing an important roll in the build up of CH_2O. The reaction had been previously overlooked because it is not needed to adequately describe methane oxidation.

A finding which is in contrast to the work of Curran et al. [16] is that no observation of the presence of formic acid (CH_2O_2) could be made. When the data of Kaiser et al. [17] was modeled against the mechanisms of Fischer et al. [15] and Curran et al. [16] with the software packages HCT and Chemkin III, general good agreement was found with a few exceptions. For lean DME flames, the intermediate hydrocarbon species mole fractions were over predicted by factors of approximately 3, with an exception being CH_2O. The model instead predicted narrower species profiles and a faster consumption of DME which, according to the authors, is a likely source of the overprediction. The final conclusion made by the authors regarding comparisons between the mechanisms and experimental data was one of overall agreement.

A final observation made by Kaiser et al. [17] is that DME will produce soot when pushed towards high equivalence ratios, but this production is still far less than that generated from comparable ethane flames.

Also from 2000 is the work of Hidaka et al. [18] who conducted high-temperature pyrolysis experiments for DME in shock waves at temperatures of 900-1900 K and pressures of 0.83-2.9 atm. The findings of this work included the determination of rate constants for five previously under-explored reactions, and the finding that the pyrolysis of DME at high

temperatures has an extremely low tendency to form higher hydrocarbons compared to hydrocarbon pyrolysis.

In 2001, Maroteaux et al. [19] conducted a "real world" investigation on the performance and emission characteristics of a four-cylinder common rail direct injection turbocharged diesel engine run on both DME and diesel fuel exclusively. The testing conditions involved the operation of the engine at the same BMEP-speed range as a conventional automotive diesel engine. Measurements were taken from exhaust before catalyst for emission of smoke, unburned hydrocarbons, NOx, and CO. The main findings were that diesel engines operated with DME will produce unburned hydrocarbons and CO if not properly tuned; however NOx emissions will remain low. Properly tuning the motor will yield a reduction in noise from the engine as opposed to when the engine is in proper tune with standard diesel fuel, the overall fuel economy is reduced due to the lower energy density of DME which requires an increased fuel consumption to maintain engine output levels.

In 2004, Qin et al. [20] developed a new optical measurement flame speed rig, and after validating their system with a few methane oxidation runs, turned their attention towards the measurement of premixed DME/air flames at pressures up to 10 atm. They found that at one atmosphere their measured flame speeds were generally in good agreement with then current DME mechanisms. The experiments conducted at elevated pressure of 2, 6, and 10 atm showed that as pressure increased the flame speed decreased considerably, with the models continually over predicting as the pressure increased. Also noteworthy was that the higher-pressure, fuel rich DME-air flames were strongly affected by hydrodynamic and thermal-diffusive instabilities.

Having noted the discrepancy between experimental data and the models, the researchers then conducted a sensitivity analysis for the mechanisms used and found that the reactions

involving the methyl and formyl radicals were playing an important role in flame propagation. The researchers' final assessment was that a systematic modification of the reaction rates associated with the production of these particular radicals would help to shore-up the discrepancies between experimental data and model.

In 2004, Zheng et al. [21] studied the ignition temperatures of nonpremixed DME flames in a counterflow device with DME concentrations ranging from 5.9-30 %, pressures ranging from 1.5 to 3.0 atm, and pressure-weighted strain rates of 110-170 s^{-1}. The researchers compared their experimental results to a 1998 DME mechanism by several authors [10,13,15,16] and a mechanism by Curran [22] which was an updated version of the 1998 mechanism. The 2003 mechanism was found to be a significant improvement over the previous version by comparing the two mechanisms against the experimental data. The researchers attributed this improvement to the updated low-temperature kinetics of the 2003 mechanism.

In 2005, Semelsberger et al [23] wrote a paper making the case for the increased use of DME as an alternative fuel. Their opening argument reasoned that DME is a non-carcinogenic, non-teratogenic, non-mutagenic, non-toxic fuel that is environmentally benign. They described the most common method of DME production which involves a two-step process of converting syngas to methanol followed by methanol dehydration to dimethyl ether, and they showed that this net reaction has an enthalpy of formation of 258.6 kJ mol^{-1}. DME can also be made from coal and biomass, and therefore its production is not limited to just one feedstock. Because the conventional route of DME production uses natural gas as the primary feedstock, they reported that the economics of DME production at present are mostly dependent on the price of natural gas. The researchers found studies which showed that the capital investment to establish the infrastructure needed to mainstream DME as a fuel in the United States would be approximately

US $4 billion, which is comparable to methanol at US $4 billion, but better than ethanol at US $5 billion, or hydrogen at a staggering US $18 billion. The capital investment for DME is comparatively low do in major part to the fact that existing LPG and natural gas infrastructures can be used for DME transportation.

Hydrogen is viewed by many as the best "end game" fuel, but according to the authors, the argument for DME as an intermediate/transitionary fuel may be a compelling one as it could be more cost effective than a step change to hydrogen. Years later, when hydrogen technologies (fuel cells, hydrogen transportation, etc.) become more advanced, DME could then be used as a hydrogen carrier.

Perhaps the most pertinent information to the work of this thesis is the author's finding that India is considering using DME-fired turbines to supply power to its southern region [24]. Asia also has an interest in DME; an estimated 105 million tons per year demand by 2010, with 50% of this being for the generation of electricity [25].

In 2005, Rosado-Reyes et al. [26] conducted flash photolysis oxidation experiments on DME at low temperatures (295-700 K) and low pressures (20-200 torr) for the purpose of studying the reactions of methoxymethyl radicals (CH_3OCH_2) with oxygen. They found two product pathways through which this can take place: the first one produces methoxymethyl peroxy radicals ($CH_3OCH_2O_2$), and the second produces OH radicals and formaldehyde (CH_2O). Transient infrared spectroscopy was used to take real-time kinetics measurements of formaldehyde, methyl formate ($HCOOCH_3$), and formic acid (CH_2O_2). From these measurements, a new temperature-dependent rate constant for methoxymethyl peroxy radical self-reaction was calculated from the kinetics of the formaldehyde and methyl formate product yields. Basically, this reaction plays a role in the kinetics of DME for temperatures below

around 650 K, and the reduction of degradation products at temperatures above this value point towards DME oxidation entering a negative temperature coefficient region. The occurrence of this phenomenon beginning at around this temperature has been pointed out by many authors previously mentioned, most notably Pfahl et al. [7]. At temperatures beyond 700 K, unimolecular decomposition reactions of DME (such as $CH_3OCH_3 \rightarrow CH_3O + CH_3$) and DME + O_2 reactions dominate the initial DME kinetics.

In 2007, Bowman et al. [27] presented an update on their ongoing efforts of assessing the effectiveness of oxygenated fuels in reducing pollutant emissions in diesel engines. The researchers had conducted shock-tube experiments to extend past the works of Pfahl et al. [7] and Dagaut et al. [9]. These experiments involved studying mixtures of DME/n-heptane for ignition times as well as providing OH time-histories. Ignition delay times for mixtures of 1% DME in Ar/O_2 had been studied at pressures of 1.8 and 3.3 atm, temperatures of 1250-1470 K, for equivalence ratios of ϕ = 0.5, 1.0, and 2.0 with the ϕ = 1.0 mixtures having the pressures extended up to 6.6 atm. The ignition delay times from these experiments were to be modeled against the latest chemical kinetics mechanism from the Lawrence Livermore National Laboratory (LLNL).

Ignition delay times for mixtures of DME/n-heptane had been obtained for ϕ = 1.0 mixtures with a total fuel mole fraction of 1% with three different DME/n-heptane ratios and at pressures of approximately 1.5 atm and temperatures of 1220-1470 K. The modeling of this particular work is done with a chemical kinetics mechanism developed through a combination of reaction and species from the LLNL DME mechanism and the LLNL reduced n-heptane mechanism [28].

Both the LLNL DME and DME/n-heptane mechanisms have been found to give good agreement with the experimental ignition delay times.

The researchers report that thus far OH time-histories have been measured in fuel rich $DME/O_2/Ar$ mixtures with $\phi \approx 3$, pressure of ~1.3 atm, and temperatures from 1400-1750 K. The major finding with these mixtures is that the LLNL model uniformly over predicts OH concentration for rich DME oxidation experiments, but does well to predict the general shape of the time-history.

In addition to the work already mentioned, experiments have been performed to measure soot formation rate and yield by a laser absorption technique for fuel rich n-heptane and DME mixtures. These mixtures were comprised of neat n-heptane (i.e., n-heptane only) and n-heptane/DME blends as fuels, with Ar gas filling the balance of the mixture. In order to make a direct comparison of the sooting characteristics these two fuel blends, the mixtures of DME/n-heptane were made with equivalent carbon atom fractions as those of the neat n-heptane mixtures. These experiments were conducted in a high-pressure shock tube facility at engine pressures (20 atm) and temperatures (1500-1900 K). At an equivalence ratio of $\phi = 5.0$, it was found that DME addition would decrease the soot yield at all times.

This study also involves the use of flow reactor data from other authors [10,15,16]. Their work is used for comparison with the LLNL mechanism which has been used throughout Bowman et al. [27].

Also in 2007, Suzaki et al. [29] used a flash/pulse photolysis technique to study low-temperature DME oxidation for mixtures of $DME/O_2/Cl_2$ from 298-600 K and pressures ranging between 20-90 torr. Time-histories of the chemical species concentrations of HO_2 and OH were measured through use of near-infrared frequency modulation spectroscopy and time-histories of

$CH_3OCH_2O_2$ were measured with UV absorption spectroscopy. The main result of this study is the inclusion of a new HCO formation pathway via QOOH (hydroperoxyalkyl) isomerization to HOQO found in the reaction OH + $CH_3OCH_2O_2$ → HO_2 + CH_3OCH_2O (methyl formate). The authors believe this reaction accounts for the fast and slow nature of HO_2 formations at various temperatures and also helps to account for the total production of CHO, which later goes on to become HO_2 and concentrations of this radical were found experimentally. A graphical explanation of this altered oxidation mechanism is provided in Fig. 3.

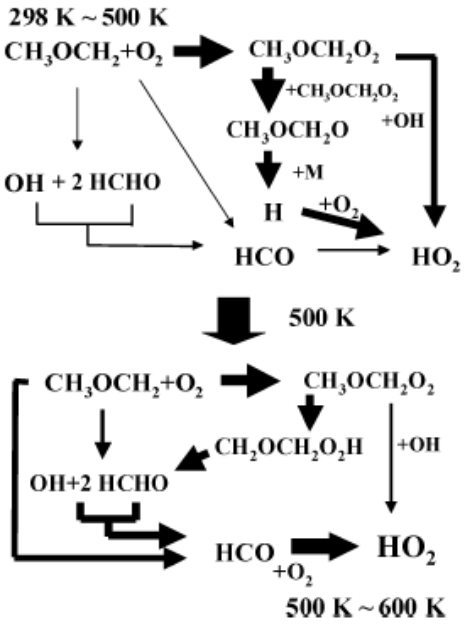

Figure 3: Schematic representation of HO2 radical formation pathways in the Cl atom initiated oxidation of DME [29].

Chen et al. [30] conducted atmospheric, room temperature, flame speed experiments for Methane/DME/Air mixtures. The experimental portions of this study included the measuring of flame speed and Markstein lengths at varying concentrations of the Methane/DME (by % volume: 100/0, 90/10, 80/20, 50/50, 0/100) at three different equivalence ratios (ϕ = 1.0, 0.8, 0.7). Observable results of these experimental flame speed measurements are that flame speed decreases with decreasing equivalence ratio while increases with increasing DME addition with

an almost linear behavior. The Markstein length and Lewis number changed dramatically at small DME concentrations.

These experimental results were compared against the models of other modeling works previously mentioned: 2000-Mech [15,16], 2003-Mech [21], 2005-Mech [22], and 2006-Mech which is a new mechanism developed by many of the authors from the current work and is presented in Zhao et al. [31]. The numerical study comparing the effectiveness of each of these mechanisms against the experimental data revealed many details: small amounts of DME addition to methane would result in a significant reduction in the high-temperature ignition delay. Investigation of radical pool growth (CH_3 and HO_2) with a computational singular perturbation analysis showed that DME addition to methane possesses a greater ignition enhancement capability than does an equivalent amount of hydrogen addition.

In the case of non-premixed methane-air systems, there was found to be two distinct ignition enhancement regimes: a kinetic-limited regime and a transport-limited regime. Of these two, the kinetic regime showed to be the most effective.

The final conclusion of their study was that the 2000-Mech, 2003-Mech, and 2005-Mech did not well reproduce the flame speed data for both DME and methane-air flames. The authors found that the 2006-Mech performed much better than these at both DME and methane-air flames, as well as with DME addition to methane.

The final major piece of this literature review is the 2007 published work for the 2006-Mech previously mentioned and presented by Zhao et al. [31]. This particular work involved experiments for DME pyrolysis at 980 K and 10 atm in a VPFR and the creation of a comprehensive high-temperature chemical kinetics mechanism for the pyrolysis and oxidation of DME.

The central effort of the modeling work was the revision of several rate constants beginning with the unimolecular decomposition reaction for DME ($CH_3OCH_3 = CH_3 + CH_3O$) by way of a theoretical study using the RRKM/master equation calculations. This provided a decomposition rate coefficient that at 1 atm is much lower (by a factor of 3 at 1000 K) than the rate constant used previously [15,16].

Another significant reaction which was modified was the H-atom subtraction reaction for the reaction of fuel with a methyl radical ($CH_3OCH_3 + CH_3 = CH_3OCH_2 + CH_4$). It was found that the rate constant for this particular reaction needed to be increased for temperatures higher than approximately 900 K. The new value is 3.5 times higher than the rate constant previously used [15,16]. Other rate constant adjustments were made based on a hierarchical methodology and included input from the recent work of other authors, species profiles collected from the VPFR experiments of their work, and more recent small molecule/radical kinetic and thermodynamic data.

The resulting chemical kinetics model was found to produce good/improved agreement with all previous relevant DME oxidation experiments, the DME/methane flame speed experiments of Chen et al. [30], and the new low-pressure burner-stabilized species profiles presented by Cool et al. [32].

CHAPTER 3: METHODOLOGY

3.1 Apparatus and procedure

As mentioned previously, significant considerations are given to the chemical kinetics of fuel oxidation when designing a gas turbine combustor. The shock tube is an ideal methodology that is well suited for the study of time-dependent, gas-phase chemical kinetics at gas turbine engine temperatures and pressures. In addition to producing the desired test conditions, shock tubes also provide the capability for a high repeatability of experiments because of their uniform flow fields. There is a rich history of the use of shock tubes for the measurement of gas-phase combustion, and more information on this topic can be found in Gaydon and Hurle [33], Bowman and Hanson [34], Bhaskaran and Roth [35], and Glass and Sislian [36]. A characteristic of shock-tube experiments which proves to be most useful for the study of homogeneous combustion processes is the near instantaneous heating of the test gas to temperatures on the order of 400 to 4000 K in a controlled environment. In the present study, shock-tube techniques are used to measure the high-temperature reaction times of potential heterogeneous gas turbine fuels at elevated temperatures and pressures.

Two shock-tube facilities were employed for the experiments detailed herein. There exists a great deal of commonality between these two facilities, particularly amongst the peripheral hardware. The first shock tube facility is located at The Aerospace Corporation in El Segundo, California. Important physical dimensions of this facility are a driven section with a length of approximately 10.7 m (35ft) and an inner diameter of 16.2 cm and a driver section 3.5 m in length with an internal diameter of 7.62 cm. An overview of this facility can be seen in Fig. 3 with a wider description of the development of this facility presented in Petersen et al.

[37]. Only the lower shock tube was used during the course of these experiments. The upper shock tube is currently undergoing modification to become its own independent system.

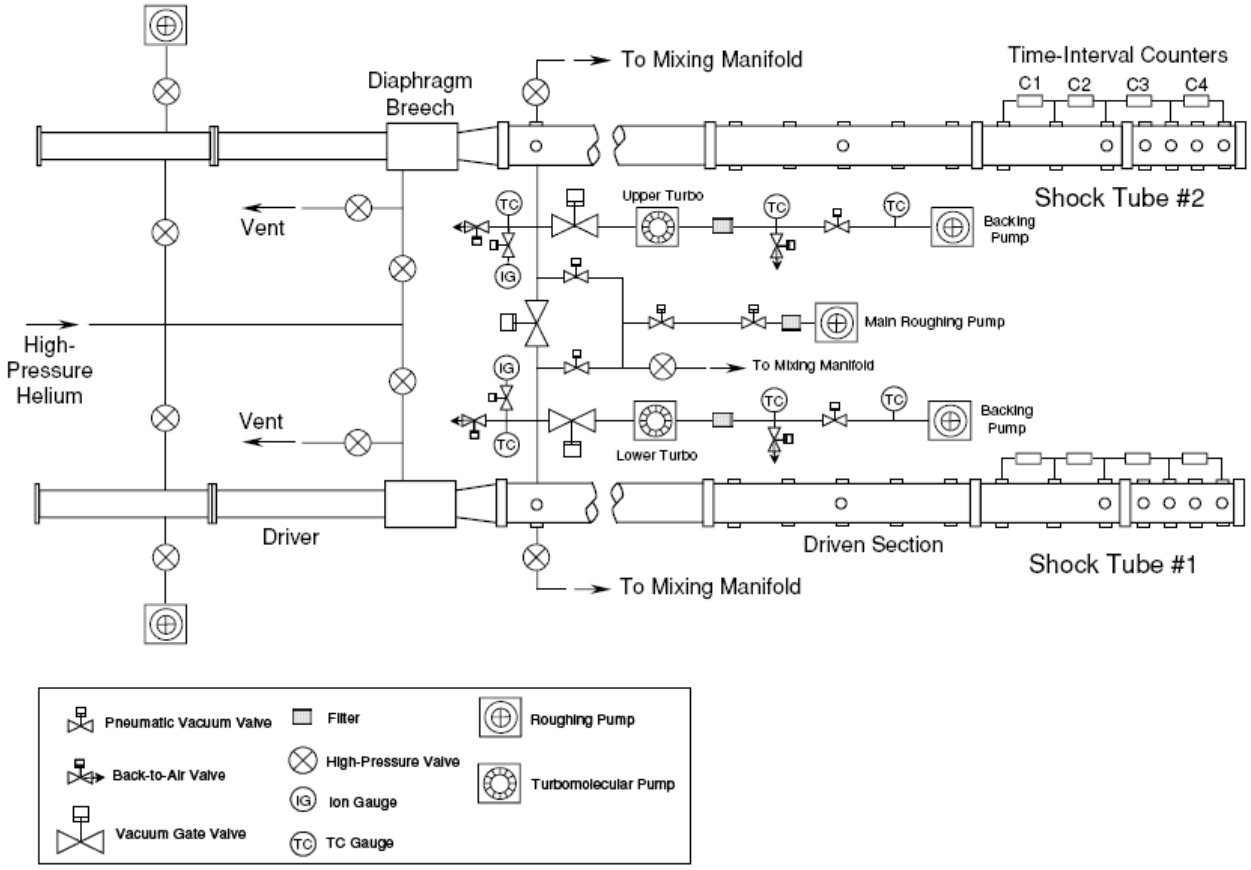

Figure 4: Schematic of the Aerospace Corporation's shock tube facility [37]. Only the lower shock tube was used in these experiments.

The second shock-tube facility was developed by the research group of Eric Petersen and its features are presented in Aul et al. [38]. Key of these features are a driven section 4.72 m in length with an internal diameter of 15.24 cm and a driver section 4.93 m long with an internal diameter of 7.62 cm. The features of this shock tube facility are presented in Fig. 5. During the course of these experiments, this shock tube was configured with both long driver and driven sections.

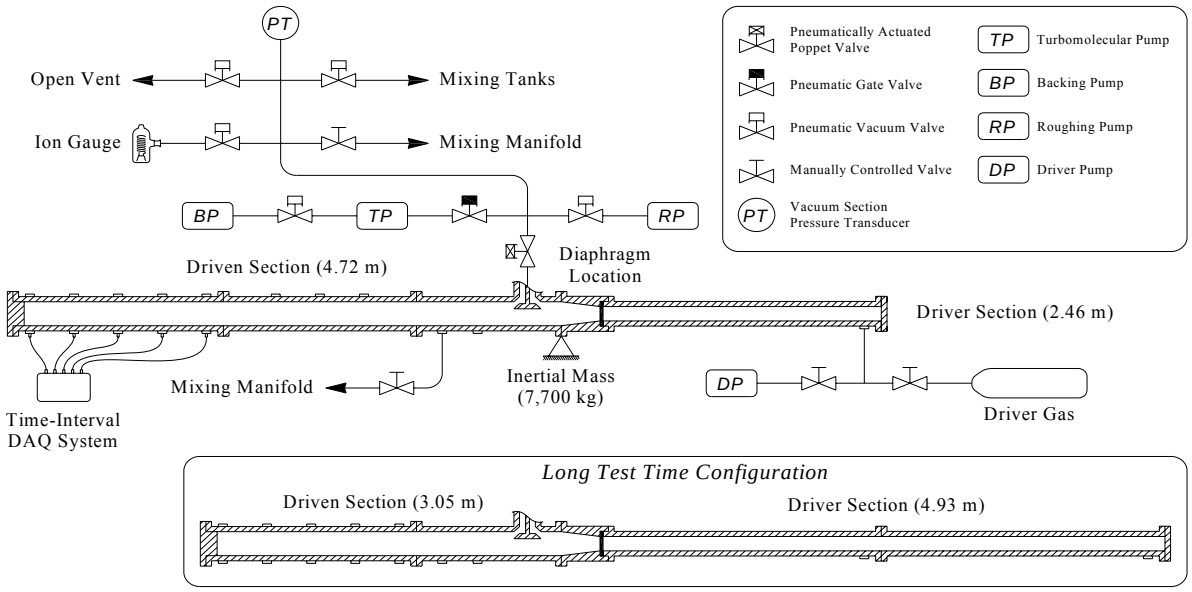

Figure 5: Schematic of the shock tube facility presented in Aul et al. [38].

As previously mentioned, both of these shock tubes have similar features and hardware. Both shock tubes are configured to generate test conditions behind reflected shocks and are capable of reflected pressures on the order of 100 atm. Untailored test times approach 3 ms. For both facilities, the conditions in the quiescent region behind the reflected shock wave are determined by one-dimensional shock relations and the incident-shock velocity. The velocity of the incident-shock is obtained by use of timer counters (Fluke PM 6666) linked to a series of sequential pressure transducers (PCB 113) at locations along the shock tube inner wall near the endwall of the driven section.

The presence of chemical reactions within the reflected-shock region is detected by piezoelectric pressure transducers (PCB 134A and Kistler 603B1) and photomultiplier tubes (Hamamatsu 1P21) mounted in custom hardware. These are located at the endwall and at a sidewall position one cm from the endwall. For the experiments conducted in this study the

activated complex CH* was of interest. To record the time history of this species, CaF_2 windows were installed at the endwall and sidewall locations and the photomultipliers were equipped with 430 ± 5 nm filters. The data acquisition for both of these shock tubes is accomplished by GageScope DAQ boards and software with sampling rates of at least 1 MHz per channel and 14-bit resolution. The endwall of both shock tubes is removable, allowing the user access to the inside of the shock tube for maintenance and cleaning. Various diaphragm-based pressure transducers are used in the filling manifolds of the driver and driven sections of both shock tubes.

The mix tanks of both shock-tube facilities are based on surplus sections of driven section tubing which are closed off at both ends by stainless steel caps and fitted with a filling "sting". The "sting" devise is a perforated 0.5-inch outer diameter stainless steel tube, fitted through the center line of the exterior side of a stainless steel mixing tank cap. This tube spans the length of the inside portion of the tank and provides a dynamic mixing effect during filling operations in preparation of creating experimental bath gas. The advantage of using a filling "sting" is that the act of charging the mix tanks immediately produces homogeneous bath gas without the extra time that would be required to obtain homogeneity through mass transfer by natural diffusion. This permits experimentation to take place soon after the mix tank charging is complete. Additional penetrations are provided for the evacuation of the mix tanks as well as for the feeding of gas mixtures into the shock tube.

The vacuum systems of both shock-tube facilities employ the use of roughing pumps, turbomolecular pumps, and backing pumps. The roughing pumps are used until a pressure of approximately 50 mTorr is achieved and at which time the roughing pump can be isolated from

the vacuum system and the turbomolecular pump can be selected to continue vacuuming out the system.

Both shock-tube facilities feature a poppet valve device which separates the vacuum sections from the shock tube. While closed, the contoured driven side of the poppet valve provides for a continuously smooth interior surface to minimize the impact on the shock wave. When opened, the poppet valve allows a larger pathway for the removal of gasses from the driven section of the shock tube, thus reducing the amount of time required to pump down the shock tube to high vacuum. Through the use of this type of system, the turbomolecular pumps of both facilities are capable of bringing their respective shock tubes to ultimate pressures on the order of 10^{-6} Torr. The plumbing of the vacuum system allows for this same system of pumps to be used to evacuate the mix tanks as well. At both facilities, ultra low pressures are measured through the use of hot cathode ion pressure gages.

In preparation for experiments, the mix tanks are evacuated to an ultimate pressure on the order of at most 10^{-6} Torr and are then closed off from the vacuum system. The fill lines which run from the supply gas bottles are now purged to ensure purity. Each gas is then metered into the mixing tank through the "sting" line to the appropriate partial pressure. Prior to the first experimental run, a small amount (2-3 psi) of the mixture is purged in order to prime the lines of the mixing manifold and to ensure that no undesired impurities enter the shock tube when filling it for an experiment.

Preparation of the shock tube for an experimental run requires ensuring a state of cleanliness in the interior of the driven section, installing optical windows in the appropriate locations, replacing the diaphragm at the interface between driver and driven sections, and sealing all sections of the shock tube. Having satisfied these things, pumping may begin on both

the driver and driven sections, now separated by a diaphragm. The driver side of both shock-tube facilities is each pumped down by roughing-style pumps. Ultra high purity is less of a requirement for the driver section. The driven sections are pumped down with both roughing and turbomolecular pumps in a manner previously described. In all of the experiment in this work, helium was used as the driver gas to rupture the diaphragm and create the incident shock wave.

3.2 Mixtures

The goal of this work was to study methane and DME oxidation in shock tubes at power generation gas turbine relevant temperatures and pressures with levels of DME concentration higher than those currently available in the literature. Studying these types of mixtures with shock tubes is a first for these particular combinations of fuels. This work was sponsored by Rolls-Royce Canada and as such, they set the terms of the experiments, i.e. what fuel mixtures and equivalence ratios were to be studied. Table 1 shows the scope of the experiments of this work.

Table 1: Mixtures and targeted pressures of this work. Temperatures are dictated by the requirement that $\tau_{ign} > 50$ μs.

Mixture #	ϕ (in "Air")	Fuel Composition (% Vol.) CH_4	Fuel Composition (% Vol.) DME	Targeted Pressures (atm)
1	2.0	80	20	20, 10, 1
2	1.0	80	20	35, 10, 1
3	0.5	80	20	20, 10, 1
4	0.3	80	20	35, 10, 1
5	2.0	60	40	20, 10, 1
6	1.0	60	40	35, 10, 1
7	0.5	60	40	20, 10, 1
8	0.3	60	40	35, 10, 1

The original plan called for experimentation at pressures of 1, 10, and 25 atm. The reasoning for alternating between a targeted pressure of 20 and 35 atm is that a suitable diaphragm was not available to produce average pressures on the order of 25 atmospheres. It was therefore decided that alternating between 20 and 35 atm for the highest pressure would be the optimal scenario and it would add a level of diversity to the data. The temperatures of these experiments were to be dictated by the requirement that ignition delay time, given as τ_{ign}, be longer than approximately 50 μs. Ignitions times faster than 50 μs typically have signal traces which are difficult to interpret due to vibration noise in the signals from the piezoelectric pressure transducers. The 50-μs limitation represents the "hot end" of the coverage for these experiments. The "cold end" would be determined as the coldest temperature which would ignite before the expansion wave reaches the test section and thermally quenches the bath gas. This occurs at approximately 2.5 ms with the Aerospace Corporation shock tube and at about 1.5 ms with the shock tube of Aul et al. using the configuration such as was previously described.

3.3 Ignition delay analysis

For these "real fuel/air" mixtures, significant pressure rises are associated with combustion, and the preferred method of data analysis is to determine the ignition delay times from data taken at the endwall. Provided in Fig. 6 are characteristic traces from an experimental run.

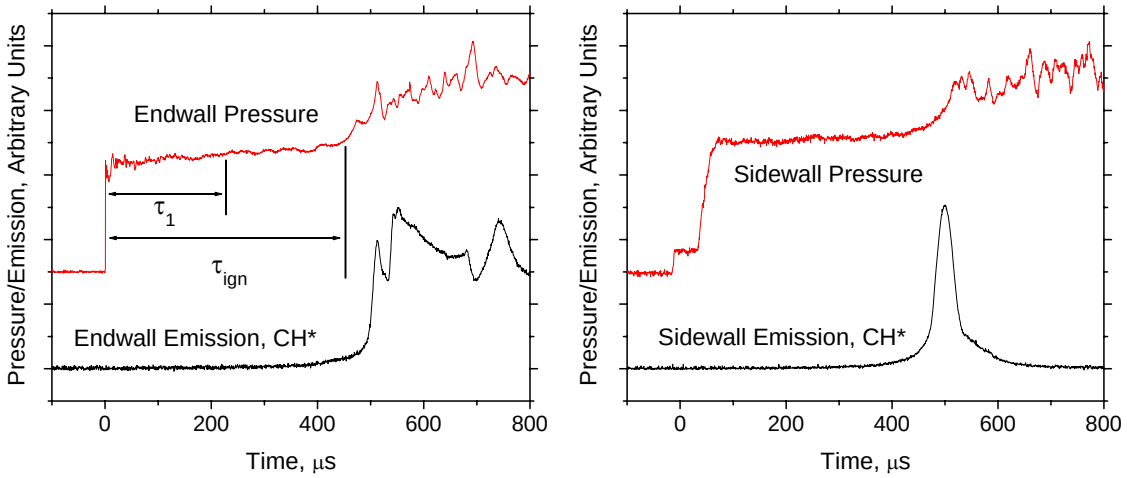

Figure 6: Emission and pressure traces for Mix #8 at P = 7.9 atm and T = 1262 K.

In the left panel are the endwall traces. The x-axis units are in μs, and the y-axis has arbitrary units. The lower, black traces are from the light emission of the activated complex CH* and the upper, red traces are pressure signals. The left panel shows these conditions at the endwall and the right panel shows them at a sidewall location 1.6 cm from the endwall.

Looking at the endwall traces, notice that time zero on the x-axis corresponds to the step increase in pressure. Pressure then begins a shallow, steady rise for several hundred microseconds until total ignition at τ_{ign} = 453 μs. The time marked by τ_1 is a point during ignition delay where chemical kinetic events have caused a rate change increase in the accumulation of pressure. The picking of this point in time plays a role later when making pressure adjustments to the final series of data.

Conditions of the reflected shock are such that ignition first begins at the endwall and then propagates away from the endwall along the axis of the shock tube. Conditions at the sidewall are also monitored because features present in endwall traces will often be found in the sidewall traces, with the sidewall offering a later temporal perspective. The endwall

photomultiplier is focused axially down the length of the shock tube and it captures emission from all of the combustion events. The sidewall sensors, with the photomultiplier focused through a narrow slit, offers a one-dimensional time history perspective of the combustion reaction.

3.4 Pressure and temperature adjustments

As was previously mentioned, τ_1 defines a point in which a significant rate change in pressure build up is occurring prior to the main ignition event. Prudence would suggest that the increased pressure and temperature occurring between the time of the reflected shock and the actual combustion event should be accounted for. Figure 7 depicts the method which is used to account for these changes in pressure and temperature.

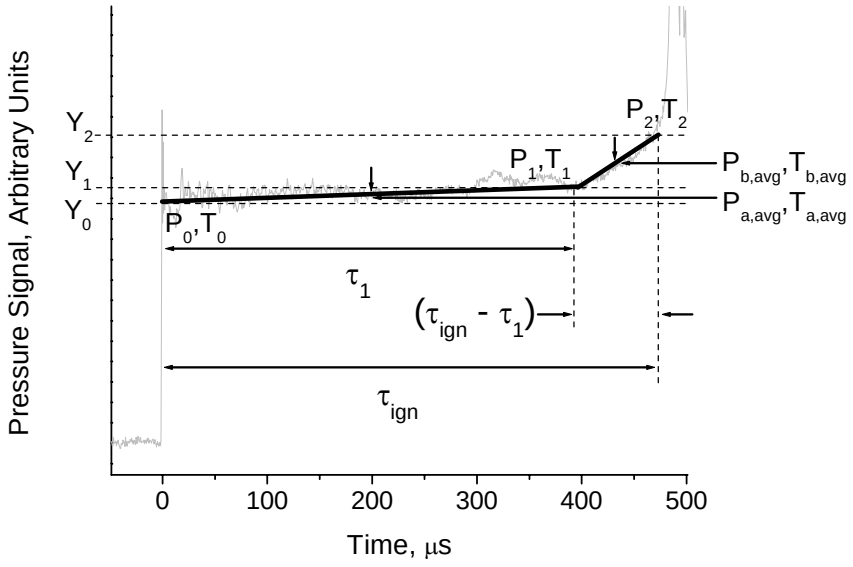

Figure 7: Explanation of pressure adjustments for a characteristic pressure trace.

An important feature of the pressure transducers is their linear calibration curves over the range of pressures seen in these shock-tube experiments. This linearity allows for the determining of pressure at any time from a known pressure at a given time. The pressure at time zero (P_0) is calculated by the program FROSH using the shock velocity and equilibrium chemistry. FROSH also provides the Temperature (T_0) and the ratio of specific heats (γ) behind the reflected wave. The calculation of pressures at other times is determined by the following relation

$$P_n = \frac{P_0}{Y_0} \cdot Y_n \tag{1}$$

And in this manner P_1 and P_2 are determined. Our interest is now turned towards obtaining the average values of pressure.

$$P_{avg} = \frac{P_n + P_{n+1}}{2} \tag{2}$$

And in this manner $P_{a,avg}$ and $P_{b,avg}$ are determined. The average value of pressure for the entire process, from time zero until ignition, should be time averaged to account for the time-dependent behavior of pressure change. The relation for determining this total process time averaged value of pressure is of the form:

$$P_{avg} = \frac{\sum_m \int P_m \cdot dt}{\int dt} \tag{3}$$

Which in this specific instance gives the following expression

$$P_{avg} = \frac{\left[P_{a,avg} \cdot \tau_1\right] + \left[P_{b,avg} \cdot \left(\tau_{ign} - \tau_1\right)\right]}{\tau_{ign}} \tag{4}$$

The other main parameter which remains to be calculated is the average temperature for this process. This follows a similar procedure to the one for calculating average pressure. The ratio of specific heats or γ is assumed to be constant for simplicity. This is a fair assumption to make because fluctuations in γ accompanying these changes in pressure (more so to the resulting changes in temperature) should be relatively small. Once again, the reflected temperature (T_0) and the ratio of specific heats (γ) are provided from the calculations of FROSH. The temperature at any time is calculated by the following relation

$$T_n = T_0 \cdot \left(\frac{P_n}{P_0} \right)^{\frac{\gamma-1}{\gamma}} \tag{5}$$

This is an adaptation of the isentropic relation for temperature and pressure in a flow with a constant ratio of specific heats. The above equation can be used to find T_1 and T_2 which correspond the pressures P_1 and P_2. The next step is the calculation of average temperatures between T_0 and T_1, T_1 and T_2.

$$T_m = \frac{T_n + T_{n+1}}{2} \tag{6}$$

And by this way $T_{a,avg}$ and $T_{b,avg}$ are determined. Finally, the time-averaged temperature for the entire process is determined by the relation

$$T_{avg} = \frac{\sum_m \int T_m \cdot dt}{\int dt} \tag{7}$$

Which for this case gives

$$T_{avg} = \frac{\left[T_{a,avg} \cdot \tau_1 \right] + \left[T_{b,avg} \cdot \left(\tau_{ign} - \tau_1 \right) \right]}{\tau_{ign}} \tag{8}$$

3.5 Correlation development

To more handily represent the data, a correlation for ignition delay is formulated. This correlation will determine ignition delay for a given temperature, pressure, and mol fraction of the chemical species considered in these experiments. It is of the general form

$$\tau_{ign} = A \cdot \prod_{i=1}^{N} \left[\frac{X_i \cdot P}{R_u \cdot T} \right]^{\nu_i} \cdot \exp\left(\frac{E_a}{R_u \cdot T} \right) \tag{9}$$

Which for our purposes becomes the following

$$\tau_{ign} = A \cdot [CH_4]^X \cdot [CH_3OCH_3]^Y \cdot [(0.21 \cdot O_2 + 0.79 \cdot N_2)_{"air"}]^Z \cdot \exp\left(\frac{E_a}{R_u \cdot T} \right) \tag{10}$$

Where τ_{ign} is the ignition delay time, A is a premulitplying constant, X_i is the mol fraction of the chemical species "i", ν_i is the power term of the chemical species "i", R_u is the universal gas constant, E_a is the activation energy of the fuel/air mixture. The bracketed terms are in units of mol per cubic centimeter.

In the form given by equation 10, there are 5 constants to be solved. This can be done handily in Microsoft Excel but first requires manipulation of the above equation. Take the natural log of equation 10 to get

$$\ln(\tau_{ign}) = \ln(A) + X \cdot \ln[CH_4] + Y \cdot \ln[CH_3OCH_3] + Z \cdot \ln[(0.21 \cdot O_2 + 0.79 \cdot N_2)_{"air"}] + \frac{E_a}{R_u \cdot T} \tag{11}$$

The next step is to compile the above terms into columns within a Microsoft Excel spreadsheet. This should include a column for $\ln(\tau_{ign})$, $\ln[CH_4]$, $\ln[CH_3OCH_3]$, ln["air"], and ln[1/T]. This should be done for all of stoichiometries to be correlated. A major caveat to this procedure is that the temperature range of experimental data to be correlated should exhibit a strong tendency towards Arrhenius kinetics, i.e. linear profiles dominate on plots of ignition

delay having a logarithmic time based y-axis and inverse temperature based x-axis. The preferred nomenclature for an Arrhenius plot is to have y-axis units in either μs or ms and x-axis units of K^{-1}. These units should carry over into the data columns being arranged for the ignition delay correlation.

The next step involves using the LINEST function with additional regression statistics. LINEST function uses the "least squares" method to calculate a strait line that best fits the data, and then returns an array that describes the line. For details on how to implement the LINEST function as an array formula, consult the Microsoft Excel Help file.

The results of this analysis will include values for the unknown constants, which provided the columns of data were created in the order given above, will be listed in the following order: E_a/R_u, Z, Y, X, and ln(A). In many text books and journal papers the preferred units for activation energy are kcal per mole. The pressure dependence of ignition delay can be estimated as pressure raised the sum of the ν_i terms.

CHAPTER 4: RESULTS

4.1 Adjustments

The intent of these experiments was to determine what effect the inclusion of high levels of Dimethyl Ether would have on the oxidation characteristics of a methane-based fuel. The targeted pressures of these experiments were 1, 10, and 25 atmospheres. Table 2 shows the pressure capabilities with the available shock-tube diaphragms.

Table 2: Available diaphragms and the range of typical reflected shock pressures each can deliver.

diaphragm thickness	diaphragm material	Pressure range
0.010 in	Polycarbonate	0.6-1.2 atm
0.020 in	Polycarbonate	1.0-1.5 atm
0.063 in	Aluminum	5-8 atm
0.085 in	Aluminum	13-20 atm
0.125 in	Aluminum	27-35 atm

The information in Table 2 set extra limitations on these experiments. It was decided that because no diaphragm in our possession would give us exactly 25-atm experiments, it would be more desirable to alternate between the 0.085 in and 0.125 in Aluminum diaphragms with the higher pressure experiments being performed for the weakest mixtures and the mixtures with equivalence ratios closest to those likely used in gas turbines, i.e. the weak $\phi = 0.3$ mixtures and the $\phi = 1.0$ mixtures. Table 3 provides a synopsis of the averaged reflected pressures obtained for each mixture.

Table 3: Average pressures obtained for each mixture.

Mixture #	ϕ (in "Air")	Fuel Composition (% Vol.) CH_4	Fuel Composition (% Vol.) DME	Targeted Pressures (atm)
1	2.0	80	20	17.5, 6.5, 1.3
2	1.0	80	20	30.5, 7.2, 1.5
3	0.5	80	20	18.5, 7.6, 1.7
4	0.3	80	20	30.6, 7.4, 1.7
5	2.0	60	40	19.2, 6.8, 1.5
6	1.0	60	40	32.2, 7.5, 1.6
7	0.5	60	40	18.8, 7.7, 1.7, 0.9
8	0.3	60	40	31.6, 7.7, 1.8

The next step was to make temperature and pressure adjustments to account for the fluctuations which occur during the time between the incident shock and the ignition event. This was done using the methods described in section 3.4. The results of these adjustments are provided in Table 4.

Table 4: Sample results of pressure and temperature adjustments. Average change in temperature for all data is 13.9 K, and average change is pressure is 0.8 atm.

	ϕ	Original Pavg (atm)	Adjusted Pavg (atm)	ΔPavg (atm)	ΔTavg (K)
Fuel Mixture: 80%CH_4 - 20%DME	2	17.5	18.4	1.0	12
		6.5	6.9	0.4	12
		1.3	1.4	0.1	15
	1	30.5	32.0	1.5	11
		7.2	7.8	0.6	20
		1.5	1.6	0.1	9
	0.5	18.5	19.4	0.9	12
		7.6	8.3	0.7	23
		1.7	1.7	0.0	8
	0.3	30.6	32.9	2.3	18
		7.4	8.0	0.5	18
		1.7	1.8	0.1	13
Fuel Mixture: 60%CH_4 - 40%DME	2	19.2	20.1	0.9	9
		6.8	7.2	0.3	11
		1.5	1.6	0.1	11
	1	32.2	34.7	2.4	16
		7.5	8.2	0.7	21
		1.6	1.7	0.1	11
	0.5	18.8	20.4	1.5	20
		7.7	8.4	0.7	23
		1.7	1.8	0.1	10
		0.9	0.9	0.0	7
	0.3	31.6	33.9	2.3	17
		7.7	8.0	0.4	14
		1.8	1.8	0.1	9

Extra runs were conducted for pressures of approximately 0.9 atm at the Aerospace Corporation for the $\phi = 0.5$, 60%CH_4 – 40%DME mixture. It was thought that these experiments would be used to duplicate the low-pressure data collected with the shock tube of Aul et al.; however, when the time came to generate these data, a thicker diaphragm was chosen in order to avoid having test pressures fall too far below one atmosphere. The results of the one atmosphere work at the Aerospace Corporation are reported in the tables above and are included in the correlations to follow.

4.2 Data plots

The preferred method of displaying ignition delay data is as a function of inverse temperature against a logarithmic time scale. This is commonly called an Arrhenius plot. The following Arrhenius plots are for the experimental data, with adjusted pressures and temperatures, and results from the correlation of adjusted data.

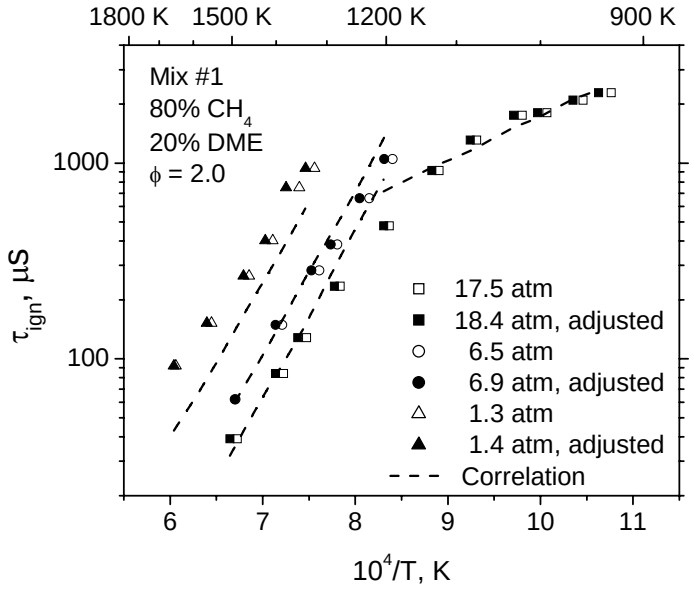

Figure 8: Ignition delay and correlation data for mix #1. Low temperature correlation under-predicts at lower pressures. All others show good agreement.

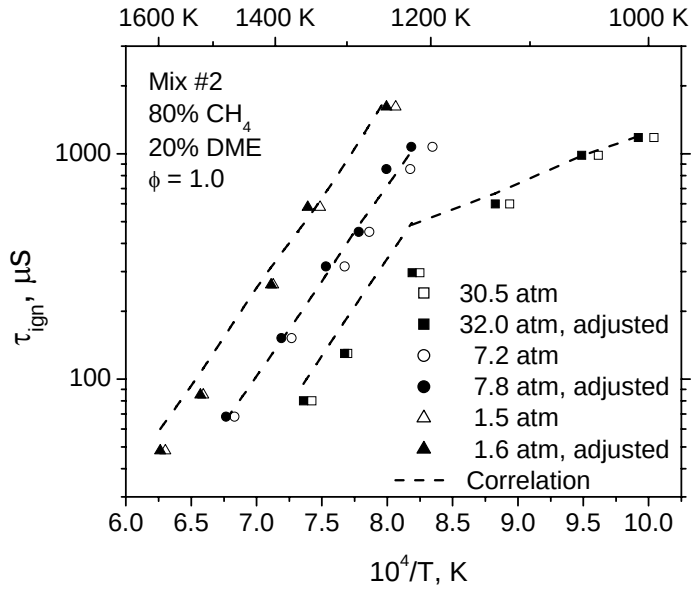

Figure 9: Ignition delay and correlation data for mix #2. Low temperature correlation over predicts high pressure data. All others show good agreement.

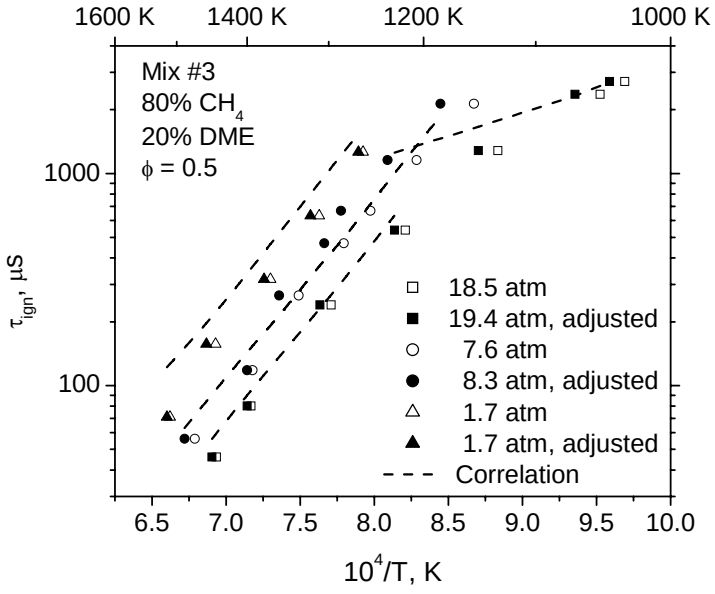

Figure 10: Ignition delay and correlation data for mix #3. The low temperature correlation makes a slight over prediction of data at lower pressures. The low temperature correlation also over predicts the data at intermediate temperatures.

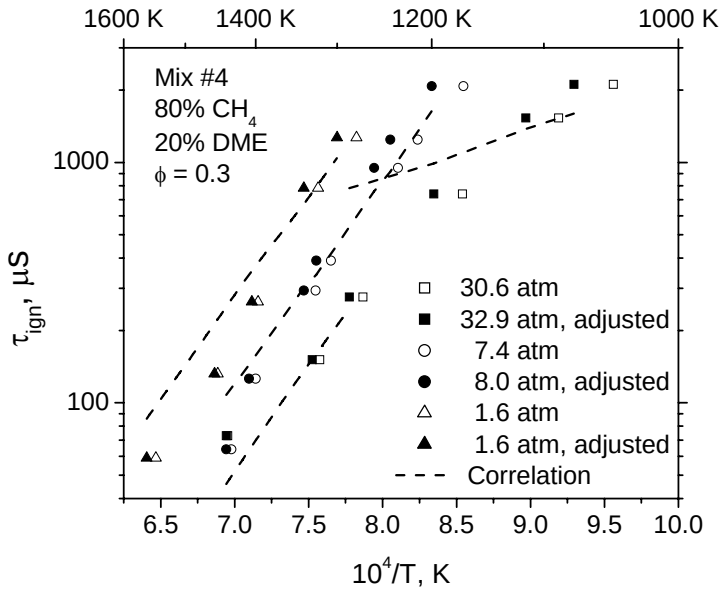

Figure 11: Ignition delay and correlation data for mix#4. The slope of the correlation curves appears to be shallower than the data. This would suggest that this lean data has higher activation energy than what is found in either the high and low temperature correlations.

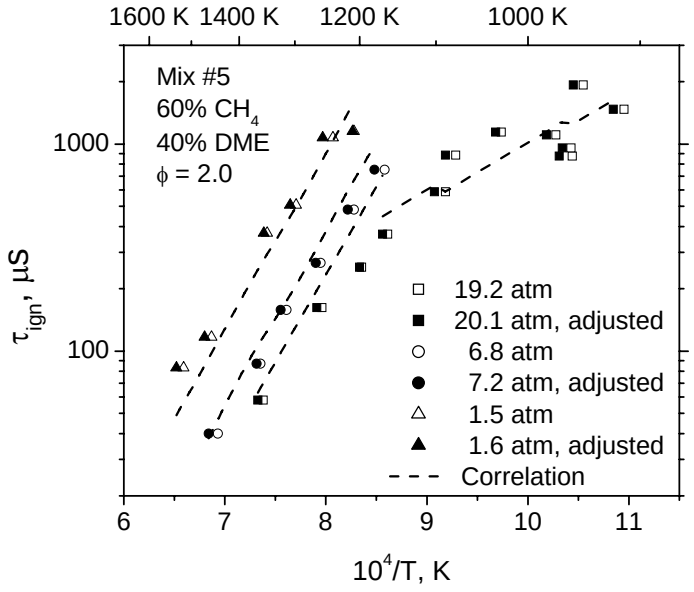

Figure 12: Ignition delay and correlation data for mix#5. There is generally good agreement between correlation and data with high temperature correlation giving some over-prediction at higher pressures. Waviness in the correlation is likely due to the fluctuations in pressure between data points.

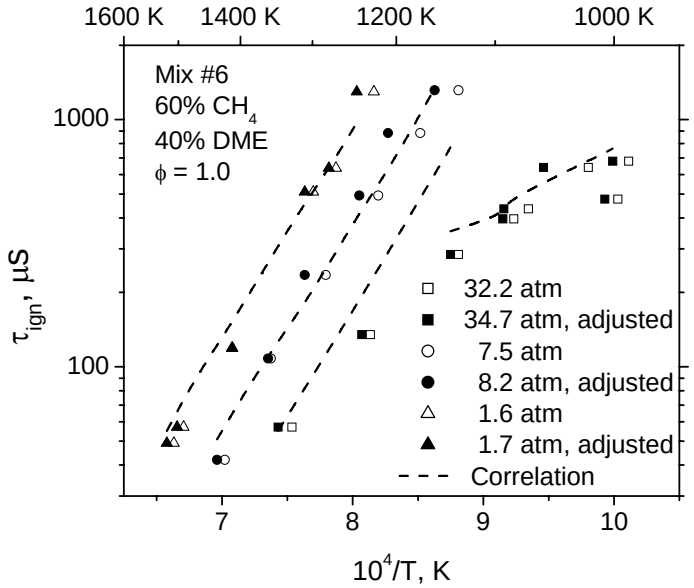

Figure 13: Ignition delay and correlation data for mix#6. Good agreement exists between high temperature correlation and two lower pressure data series, but the correlation tends to over-predict at higher pressures. The Lower temperature correlation does a fair job predicting ignition delay.

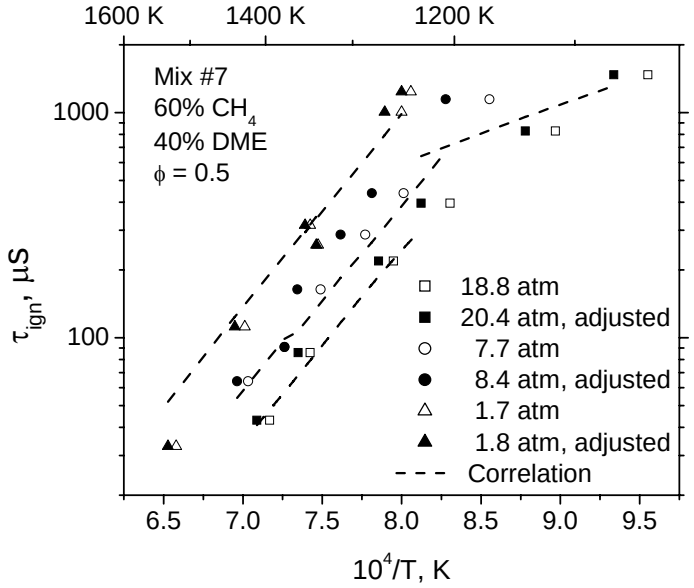

Figure 14: Ignition delay and correlation data for mix#7. The high temperature correlation tends to under predict the mid range and high pressure data, while the low temperature correlation appears to have an activation energy which is lower than that of the data.

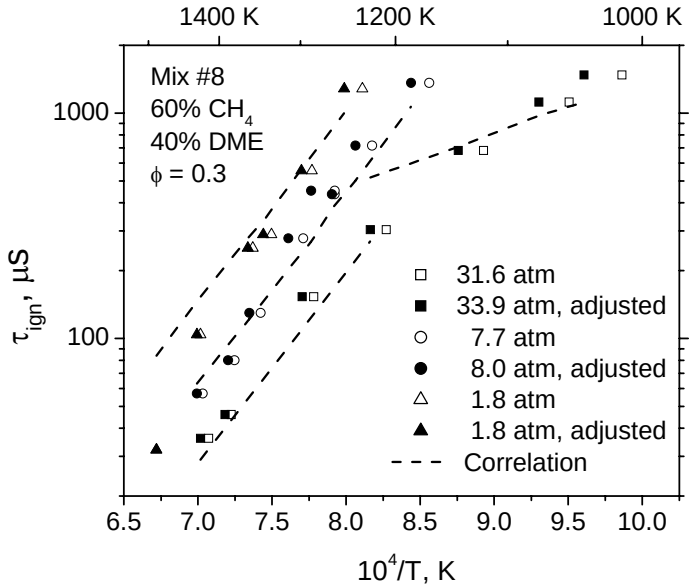

Figure 15: Ignition delay and correlation data for mix#8. The high temperature correlation appears to be in fair agreement with the data while the low temperature correlation seems to have an activation energy which is too low for this data.

Overall, the two correlations perform well – showing good agreement with the majority of data from these experiments. The high-temperature correlation does tend to have some difficulty predicting low-pressure ignition delay by over-predicting at the fuel lean equivalence ratios and under-predicting the fuel rich. The correlation does exceptionally well at $\phi = 1.0$ for the lower pressures. At intermediate pressures, the high-temperature correlation performs fairly well with the few exceptions being the fuel lean mixtures containing higher concentrations of DME.

In most all cases, the high-temperature correlation tends to over-predict the high-pressure data, especially near the low-temperature limit. The few exceptions to this are the fuel lean mixtures containing higher concentrations of DME. The likely reason for this over-prediction appears to be a change in the activation energy for many mixtures in the vicinity of 1250 K. A solution to this problem may be to extend the temperature coverage of this correlation into cooler

temps. A drawback to this approach might be larger discrepancies between the correlation and lower pressure data. A second alternative would be to separate the data between low and high pressures, with one high-temperature correlation providing coverage for pressures below approximately ten atmospheres, and a second high-temperature correlation for pressures above ten atmospheres. The present correlation appears to be sufficient enough to provide combustion researchers with a "good estimate" as to what they should expect for mixtures of this type, and as such, no further changes to it will be made.

The low temperature correlation's discrepancies with the data appear to be centered on a difference in activation energy between the stoichiometric/fuel rich and fuel lean mixtures. The correlation seems to exhibit a bias towards the activation energy of the stoichiometric/fuel rich mixtures. This is likely the result of an over abundance in stoichiometric/fuel rich data compared to the relatively fewer data for fuel lean mixtures. Even with the differences as they are, this correlation does provide good-to-fair agreement with the majority of data for which it is intended and no further adjustments to this correlation will be made.

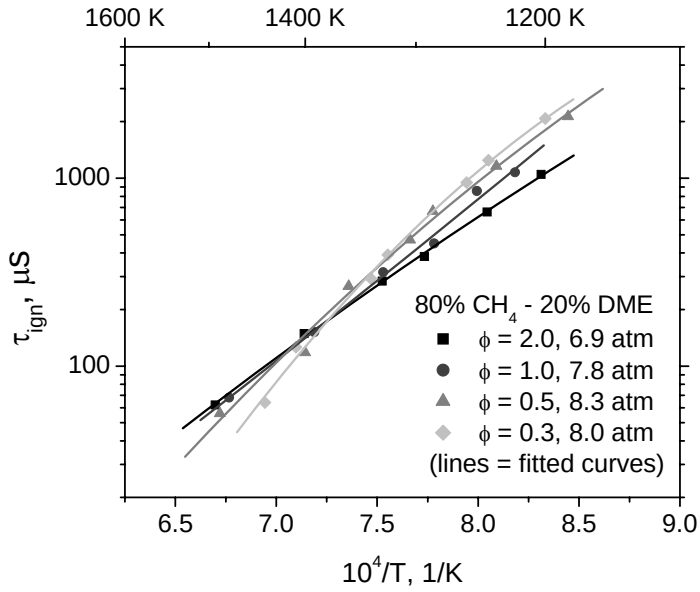

Figure 16: Comparison of equivalence ratios for ignition delay data of 80%CH_4 – 20%DME mixtures with similar adjusted temperatures and pressures. Data show similar ignition delay between 1370-1425 K.

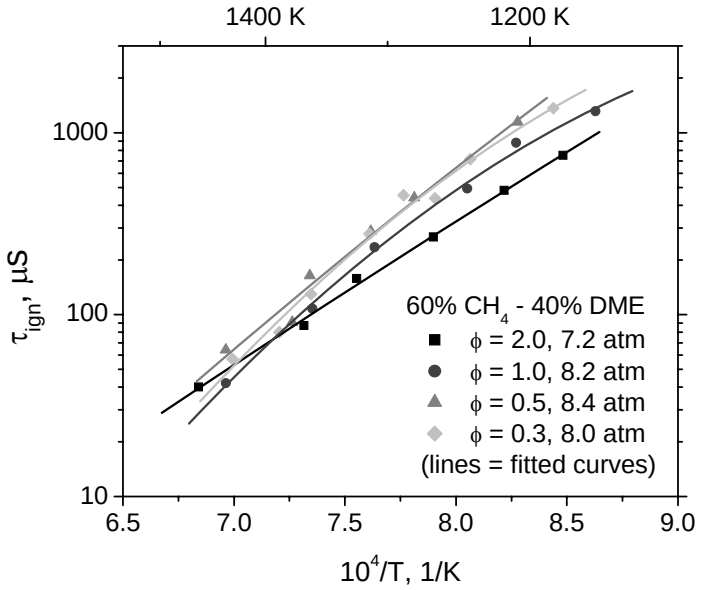

Figure 17: Comparison of equivalence ratios for ignition delay data of 60%CH_4 – 40%DME mixtures with similar adjusted temperatures and pressures. Stoichiometric and rich data cross at approximately 1390 K; lean data merge at temperatures ranging from 1230-1350 K.

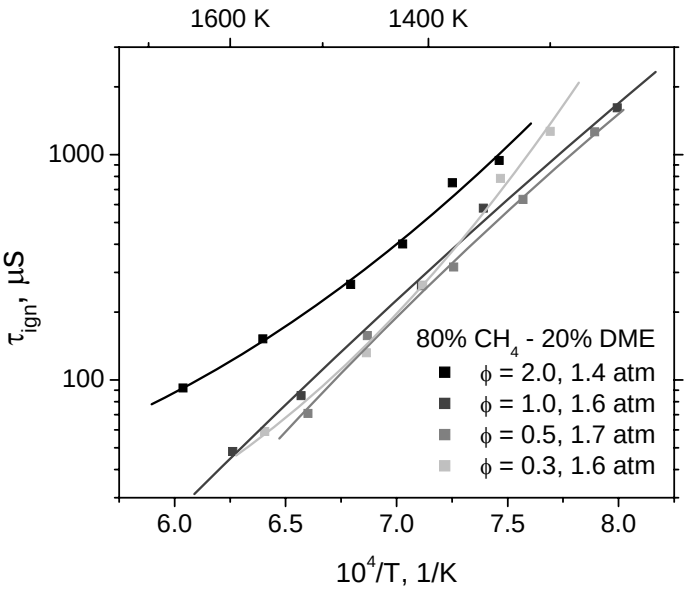

Figure 18: Ignition delay data for 80%CH_4 – 20% DME mixtures with similar adjusted temperatures and pressures. The fuel rich mixture is the slowest to ignite while the others are similar for T > 1400 K.

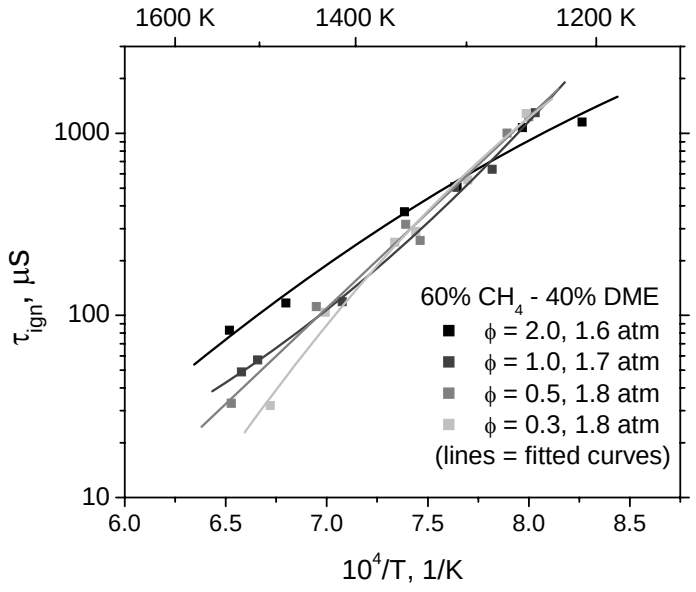

Figure 19: Ignition delay data for 60%CH_4 – 40%DME mixtures with similar adjusted temperatures and pressures. The fuel rich mixture is the slowest of the four equivalence ratios at temperatures hotter than 1300 K, but becomes the fastest for temperatures less than 1275 K.

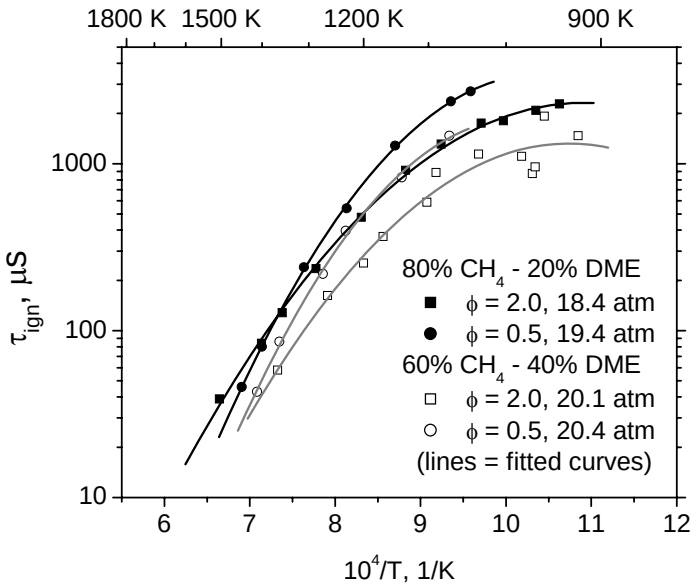

Figure 20: Comparison of fuel mixtures with ignition delay times for ϕ = 2.0, 0.5 mixtures with similar adjusted temperatures and pressures. The differences in mixtures are more pronounced at cooler temperatures.

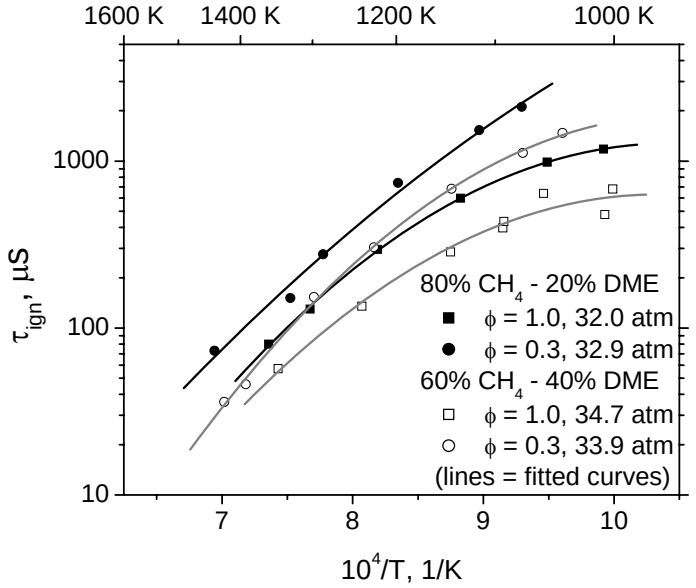

Figure 21: Comparison of fuel mixtures with ignition delay times for ϕ = 1.0, 0.3 mixtures with similar adjusted temperatures and pressures. The ϕ = 1.0 mixture of the 80/20 mix has an ignition delay profile similar to that of the 60/40 ϕ = 0.3 mixture.

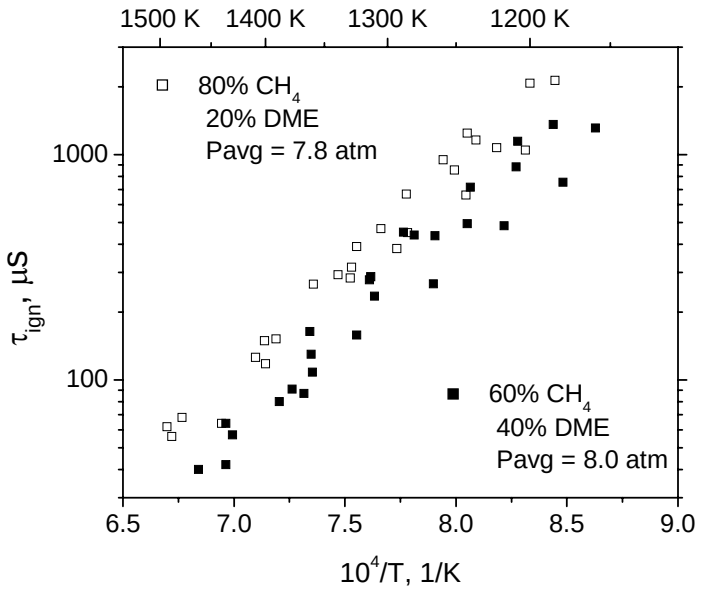

Figure 22: Comparison of mixtures for similar adjusted pressures and temperatures. With a few exceptions, the mixture having the greatest concentration of DME has the faster ignition times.

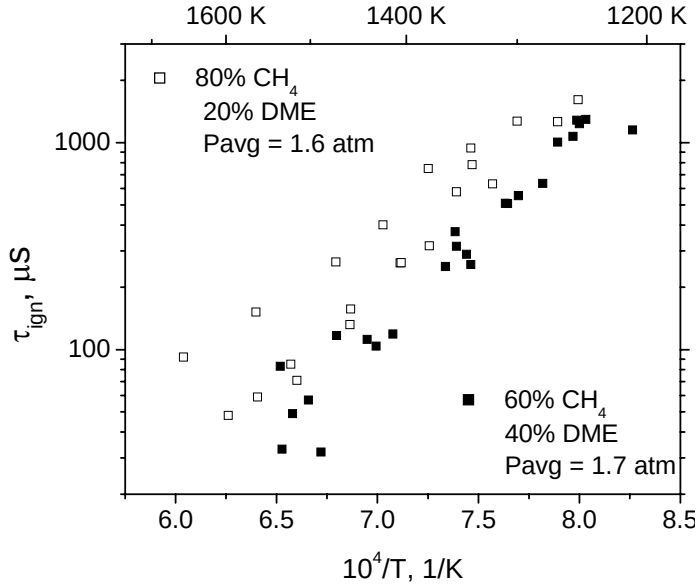

Figure 23: Comparison of mixtures of similar adjusted pressures and temperatures. In much the same way as Fig. 25, the mixture which contains the higher concentration produces the faster ignition time.

In Figs. 16 and 17 are ignition delay times for mixtures of the same fuel type. These mixtures are again presented in Fig. 22. Comparing these three figures reveals that an increase in

DME concentration will result in consistently faster ignition times with little dependence upon equivalence ratio. For mixtures at these pressures (approximately 7-8 atm) there is a transition temperature at approximately 1400 K where relatively fast mixtures become relatively slow mixtures. In this case, the fuel lean mixtures are faster at temperatures greater than approximately 1400 K and at temperatures colder than 1400 K they become the slower mixtures.

A similar phenomenon is seen occurring in Figs. 18, 19, and 23. Again, the higher concentrations of DME consistently produce faster ignition times. The transition phenomenon is also present as well, but occurs at a colder temperature (approximately 1300 K) and is only well pronounced in the 60%CH_4 – 40%DME fuel mixtures.

Figures 20 and 21 compare the two fuel mixtures at elevated pressures. Both figures share a common thread in that the richest 80%CH_4 – 20%DME mixture and the leanest 60%CH_4 – 40%DME mixture have similar ignition delay times. At these elevated pressures, the slope of the ignition plots begins to shallow out as the temperatures become colder. This indicates the possibility for negative temperature coefficient regions at temperatures colder than those examined in this work.

4.3 Correlation

Two ignition delay time correlations were formulated by using the correlation methods of section 3.5 with experimental data adjusted for pressure and temperature by the methods described in section 3.4. The first correlation is for temperatures of at least 1175 K and pressures ranging from 0.8 to 35.3 atm. Units of ignition delay are μs and the units of activation energy are kcal per mole.

$$\tau_{ign} = \left(2.16\times10^{-8}\right)\cdot\left[CH_4\right]^{0.550}\cdot\left[DME\right]^{-0.710}\cdot\left["Air"\right]^{-0.432}\cdot\exp\left(42.8/R_u\cdot T\right) \qquad (12)$$

The overall pressure dependency of this correlation is on the order of $P^{-0.59}$. This correlation shows us that ignition delay behavior will become longer with increased methane concentration. This is indicated by the methane terms positive exponent. Alternately, the DME and "Air" terms, with their negative exponents, will advance the onset of ignition in instances where either of these concentrations is increased. A comparison between ignition delay times from this correlation and those of the adjusted data can be seen in Fig. 24.

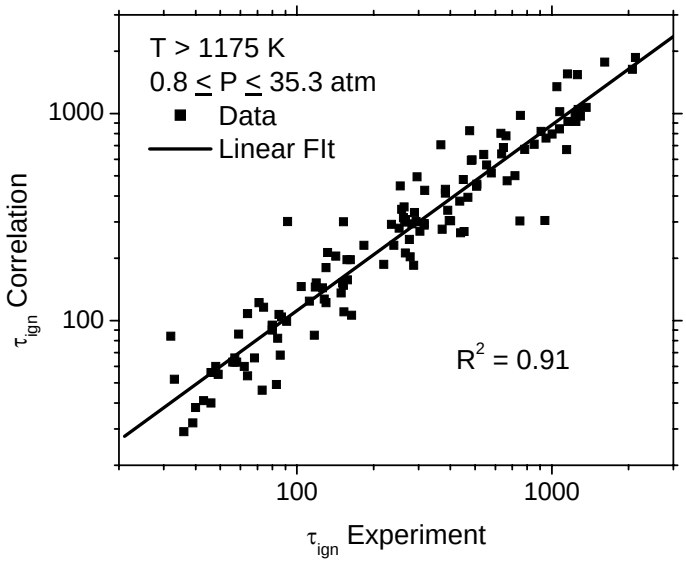

Figure 24: Parity plot for experimental results against the high temperature correlation. Ignition times in μs.

The second correlation is for temperatures less than 1175 K and pressures ranging from 18.5 to 40.0 atm. Units of ignition delay are μs and the units of activation energy are kcal per mol.

$$\tau_{ign} = \left(2.27 \times 10^{-6}\right) \cdot \left[CH_4\right]^{0.098} \cdot \left[DME\right]^{-0.775} \cdot \left["Air"\right]^{-0.0541} \cdot \exp\left(15.6/R_u \cdot T\right) \qquad (13)$$

The pressure dependence of the above correlation is on the order of $P^{-1.22}$. Again, it can be seen that increased methane concentrations will tend to slow the onset of ignition and increasing either DME or "Air" will hasten the ignition delay times. At these cooler temperatures it is

worthwhile to note that the overall impact of adjusting the levels of methane or "Air" is much less than is seen with the high-temperature correlation. A comparison between ignition delay times from this correlation and those of the adjusted data can be seen in Fig. 25.

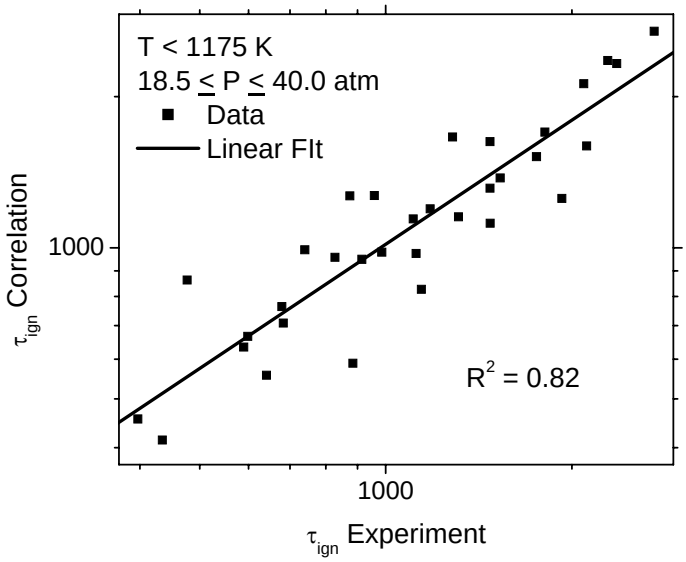

Figure 25: Parity plot for experimental results against the low temperature correlation. Ignition times in μs.

The low pressure series (≤ 1 atm) of data taken at the Aerospace Corporation differs from the low pressure data (≈ 1.8 atm) taken with the facility of Aul et al. by approximately 0.9 atm. This difference in pressure creates a significant difference in ignition delay time. In order to make a better comparison between data taken at these two facilities, the pressure dependence of the high temperature correlation can be used to scale the ignition delay data of either series. Figure 26 presents the results of pressure scaling for ignition delay times conducted for the 60%CH_4 – 40%DME fuel mixtures from the Aerospace Corporation with equivalence ratios of $\phi = 0.5$.

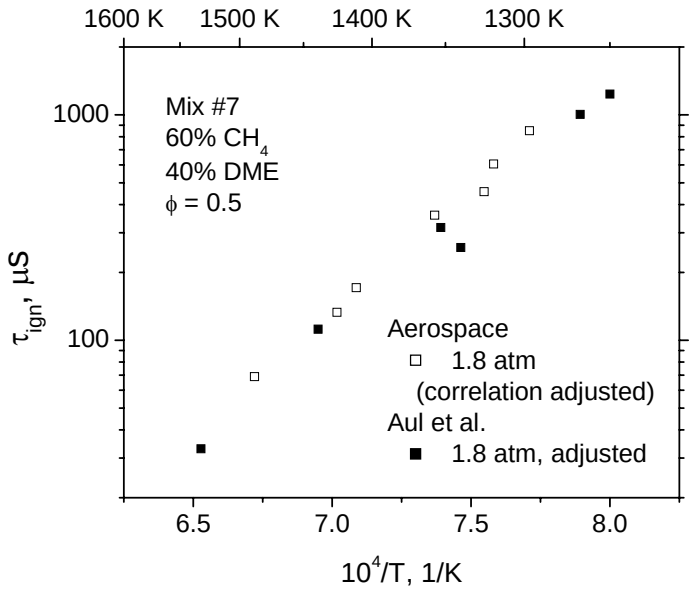

Figure 26: Comparison of data from both shock tube facilities. Pressure adjustments for ignition delay times from the high temperature correlation allow a better comparison of these two data series.

CHAPTER 5: CONCLUSIONS AND RECOMMENDATIONS

5.1 Conclusions

The decision to make changes to the targeted pressures of the original experimental matrix turned out to be for the better. The pressure diversity has allowed for the creation of two ignition correlations which now span a greater range of conditions than likely would have been possible had the original matrix been followed (pressures up to 40 atm compared to what would have likely been a maximum of 28-30 atm). The findings of this work include that at pressures below ten atmospheres, an increased level of dimethyl ether will consistently produce faster ignition in a methane-based fuels. At pressures above approximately ten atmospheres, this may not be the case, especially towards colder temperatures where it may be possible for fuel rich mixtures with lower concentrations of dimethyl ether to produce faster ignition times.

An interesting characteristic of methane and dimethyl ether oxidation that has not been given much attention in the literature is the tendency for these mixtures to release energy for long periods of time prior to ignition. The fact that adjustments for temperature and pressure were required in order to more accurately establish conditions at the time of ignition is a requirement not typical of the other methane-based fuels that the author and his coworkers have previously studied.

5.2 Recommendations

The study of high-temperature oxidation of these fuels provides valuable information for those involved in dimethyl ether development as a fuel additive and alternative fuel. It could also be worthwhile to further investigate the low-temperature, high-pressure oxidation

characteristics of these fuels. There is a very real possibility that negative temperature coefficient regions exist at temperatures just beyond those studied in this work. It would also be of interest to further pursue the issue of data scatter in the fuel rich, high-pressure mixtures. It may be possible that this phenomenon is somehow linked to the flame propagation instabilities noted by Qin et al. [20] in their high-pressure, fuel rich flame speed work.

APPENDIX: TABULATED DATA

(Mix#1) ϕ = 2.0	Temp. (K)	Press. (atm)	τ_{ign}, (μs)	Adjusted Press. (atm)	Adjusted Temp. (K)	High Temp. Cor. (μs)	Low Temp Cor. (μs)
	1487	12.4	39	13.2	1505	32	
	1384	13.8	84	14.8	1401	82	
	1338	15.4	128	16.5	1355	127	
	1276	15.6	235	16.2	1286	291	
	1195	17.0	477	17.7	1204	825	
	1123	17.7	915	18.5	1133		948
	1074	18.9	1311	19.7	1082		1153
	1020	19.1	1754	20.1	1030		1519
	993	20.2	1809	21.2	1003		1699
	956	20.5	2091	21.7	966		2121
	929	21.6	2287	23.1	941		2361
	1491	5.4	62	5.4	1493	60	
	1387	5.9	149	6.2	1401	136	
	1314	6.3	283	6.7	1329	293	
	1281	6.9	383	7.2	1293	430	
	1227	7.2	662	7.8	1243	781	
	1190	7.5	1049	8.0	1203	1349	
	1650	0.9	92	1.0	1656	43	
	1551	1.1	152	1.2	1563	79	
	1459	1.3	265	1.3	1472	167	
	1407	1.3	401	1.4	1423	258	
	1352	1.4	749	1.6	1379	390	
	1323	1.5	941	1.7	1340	588	

(Mix#2) ϕ = 1.0	Temp. (K)	Press. (atm)	τ_{ign}, (μs)	Adjusted Press. (atm)	Adjusted Temp. (K)	High Temp. Cor. (μs)	Low Temp Cor. (μs)
	1347	26.0	80	27.2	1359	95	
	1299	27.7	130	28.2	1303	180	
	1212	30.0	296	31.1	1221	495	
	1119	31.6	598	33.5	1133		666
	1040	32.5	985	34.7	1054		980
	996	35.2	1180	37.2	1008		1195
	1464	6.1	68	6.4	1478	66	
	1376	6.8	152	7.2	1391	148	
	1303	7.0	316	7.7	1328	289	
	1272	7.5	450	7.9	1285	479	
	1223	7.7	854	8.6	1251	711	
	1198	8.1	1074	8.9	1222	1021	
	1587	1.3	48	1.3	1597	60	
	1517	1.4	85	1.4	1522	107	
	1403	1.5	262	1.5	1406	314	
	1336	1.6	579	1.8	1353	517	
	1240	1.7	1614	1.8	1251	1774	

(Mix#3) ϕ = 0.5	Temp. (K)	Press. (atm)	τ_{ign}, (μs)	Adjusted Press. (atm)	Adjusted Temp. (K)	High Temp. Cor. (μs)	Low Temp Cor. (μs)
	1442	15.6	46	15.9	1448	56	
	1395	16.2	80	16.4	1400	90	
	1297	17.6	240	18.5	1310	231	
	1218	18.6	541	19.5	1229	634	
	1132	19.5	1283	20.8	1149		1662
	1050	20.6	2366	22.3	1069		2327
	1032	21.4	2719	22.4	1043		2700
	1473	6.5	56	6.8	1488	63	
	1393	7.1	118	7.3	1400	145	
	1335	7.5	266	8.2	1359	212	
	1283	7.6	469	8.3	1305	394	
	1254	8.1	668	9.1	1286	473	
	1207	8.2	1159	9.1	1236	915	
	1153	8.4	2133	9.5	1184	1865	
	1510	1.4	71	1.5	1515	122	
	1443	1.6	157	1.7	1456	197	
	1370	1.7	317	1.8	1378	425	
	1311	1.8	632	1.8	1321	803	
	1262	1.8	1261	1.8	1267	1541	

(Mix#4) ϕ = 0.3	Temp. (K)	Press. (atm)	τ_{ign}, (μs)	Adjusted Press. (atm)	Adjusted Temp. (K)	High Temp. Cor. (μs)	Low Temp Cor. (μs)
	1438	28.2	73	28.4	1440	46	
	1320	28.0	151	28.8	1329	152	
	1271	29.5	276	31.0	1286	246	
	1171	31.2	740	34.4	1198		991
	1088	32.6	1532	36.4	1115		1377
	1046	34.1	2114	38.5	1076		1596
	1433	6.7	64	6.8	1440	108	
	1400	7.0	126	7.2	1409	144	
	1325	7.2	293	7.6	1339	301	
	1307	7.6	391	8.1	1324	341	
	1234	7.6	949	8.3	1259	760	
	1214	7.9	1244	8.8	1242	916	
	1170	8.0	2075	8.9	1200	1635	
	1546	1.5	59	1.5	1561	86	
	1452	1.6	132	1.6	1457	213	
	1397	1.6	263	1.7	1405	354	
	1322	1.8	783	1.9	1339	672	
	1278	1.9	1269	2.0	1300	1045	

(Mix#5) ϕ = 2.0	Temp. (K)	Press. (atm)	τ_{ign}, (μs)	Adjusted Press. (atm)	Adjusted Temp. (K)	High Temp. Cor. (μs)	Low Temp Cor. (μs)
	1355	14.2	58	14.8	1365	63	
	1256	16.2	162	16.8	1264	197	
	1197	18.3	254	18.6	1200	447	
	1161	18.8	367	19.4	1168	706	
	1089	17.9	589	19.1	1102		634
	958	19.7	875	21.1	970		1269
	1077	20.3	885	21.6	1089		589
	959	20.6	959	21.5	967		1270
	973	20.3	1108	21.4	982		1142
	1027	20.6	1142	21.3	1033		827
	913	22.0	1474	23.1	922		1627
	948	21.7	1928	22.9	957		1254
	1443	5.8	40	6.3	1462	38	
	1360	6.0	87	6.2	1367	104	
	1314	6.7	158	7.0	1324	157	
	1258	7.3	267	7.6	1266	308	
	1208	7.4	483	7.7	1217	593	
	1165	7.7	753	8.3	1179	981	
	1517	1.3	83	1.4	1534	49	
	1456	1.3	117	1.4	1471	85	
	1348	1.5	371	1.5	1354	276	
	1298	1.6	507	1.7	1308	445	
	1239	1.6	1073	1.8	1255	843	
	1208	1.8	1152	1.8	1210	1555	

(Mix#6) ϕ = 1.0	Temp. (K)	Press. (atm)	τ_{ign}, (μs)	Adjusted Press. (atm)	Adjusted Temp. (K)	High Temp. Cor. (μs)	Low Temp Cor. (μs)
	1327	28.0	57	30.1	1346	55	
	1229	32.2	135	33.6	1239	194	
	1135	34.1	285	35.3	1143	774	
	1083	33.9	397	35.5	1093		456
	1070	34.9	435	38.6	1092		414
	997	30.5	477	32.1	1007		862
	1020	29.9	641	35.5	1057		557
	989	34.4	679	36.5	1001		763
	1424	6.5	42	6.8	1436	51	
	1356	7.0	108	7.1	1360	110	
	1283	7.3	235	8.1	1310	182	
	1220	8.1	493	8.9	1242	415	
	1174	8.2	882	9.4	1209	631	
	1135	8.2	1314	9.1	1159	1338	
	1508	1.5	49	1.5	1520	55	
	1491	1.4	57	1.5	1502	66	
	1412	1.6	119	1.6	1413	152	
	1299	1.7	509	1.7	1310	456	
	1270	1.8	636	1.9	1279	638	
	1225	1.8	1295	2.0	1245	971	

(Mix#7) ϕ = 0.5	Temp. (K)	Press. (atm)	τ_{ign}, (μs)	Adjusted Press. (atm)	Adjusted Temp. (K)	High Temp. Cor. (μs)	Low Temp Cor. (μs)
	1395	16.0	43	16.9	1411	41	
	1347	17.1	86	18.0	1361	68	
	1258	18.5	219	19.5	1273	187	
	1204	20.0	396	22.1	1231	304	
	1115	20.3	828	22.4	1139		957
	1047	21.0	1474	23.3	1071		1314
	1422	6.8	64	7.1	1436	54	
	1377	7.1	91	7.1	1377	99	
	1335	7.7	164	8.4	1362	106	
	1287	7.8	287	8.5	1313	185	
	1248	8.3	439	9.3	1280	265	
	1169	8.5	1145	10.0	1208	669	
	1482	0.8	74	0.8	1488	116	
	1415	0.9	142	0.9	1425	205	
	1398	0.9	183	0.9	1411	231	
	1345	0.9	383	0.9	1357	412	
	1322	0.9	487	0.9	1325	597	
	1316	0.8	647	0.8	1319	685	
	1292	1.0	908	1.0	1297	820	
	1520	1.6	33	1.7	1532	52	
	1426	1.6	112	1.7	1439	124	
	1338	1.8	258	1.8	1340	345	
	1347	1.8	316	1.8	1353	294	
	1250	1.8	1004	1.9	1267	795	
	1241	1.9	1235	2.0	1250	988	

(Mix#8) ϕ = 0.3	Temp. (K)	Press. (atm)	τ_{ign}, (μs)	Adjusted Press. (atm)	Adjusted Temp. (K)	High Temp. Cor. (μs)	Low Temp Cor. (μs)
	1414	26.8	36	27.7	1425	29	
	1384	27.6	46	28.3	1392	40	
	1285	30.0	153	31.5	1298	110	
	1209	33.1	304	35.1	1225	270	
	1120	33.8	683	37.0	1142		708
	1052	34.5	1120	38.0	1075		974
	1014	35.7	1476	40.0	1041		1119
	1422	6.7	57	6.9	1430	63	
	1380	7.0	80	7.2	1388	94	
	1347	7.4	130	7.7	1361	122	
	1297	7.7	278	8.1	1314	203	
	1262	7.9	436	8.0	1265	378	
	1262	7.9	453	8.7	1288	269	
	1223	8.2	717	8.7	1240	501	
	1168	8.4	1363	9.0	1185	1070	
	1488	1.6	32	1.6	1488	84	
	1425	1.6	104	1.6	1430	146	
	1357	1.8	252	1.8	1363	279	
	1334	1.9	289	2.0	1344	332	
	1287	1.9	555	2.0	1299	564	
	1233	1.9	1283	2.1	1252	999	

LIST OF REFERENCES

[1] A.H. Lefebvre, 1999, "Gas Turbine Combustion", 2nd Ed, Taylor and Francis, New York, NY.

[2] R.M. Flores, M.M. Miyasato, V.G. McDonell, and G.S. Samuelsen, 2001, "Response of a Model Gas Turbine Combustor to Variation in Gaseous Fuel Composition", ASME J. Eng. Gas Turbines Power, **123**, pp 823-831.

[3] L.J. Spadaccini, and M.B. Colket, 1994, "Ignition Delay Characteristics of Methane Fuels", Prog. Energy Combust. Sci., **20**, pp 432-460.

[4] E.L. Petersen, D.F. Davidson, and R.K. Hanson, 1999, "Kinetics Modeling of Shock-Induced Ignition in Low-Dilution CH4/O2 Mixtures at High Pressures and Intermediate Temperatures", Combust. Flame, **117**, pp 272-290.

[5] J. Huang, P.G. Hill, W.K. Bushe, and S.R. Munshi, 2004, "Shock-Tube Study of Methane Ignition Under Engine-Relevant Conditions: Experiments and Modeling", Combust. Flame, **136**, pp 22-42.

[6] G. Bourque, D. Healy, H. Curran, C. Zinner, D. Kalitan, J. deVries, C. Aul, and E. Petersen, "Ignition and Flame Speed Kinetics of Two Natural Gas Blends with High Levels of Heavier Hydrocarbons", Proc. ASME Turbo Expo, June 9-13, Berlin, Germany, (submitted).

[7] U. Pfahl, K. Fieweger, and G. Adomeit, 1996, "Self-Ignition of Diesel-Relevant Hydrocarbon-Air Mixtures Under Engine Conditions", Twenty-Sixth Symposium (International) on Combustion, The Combustion Institute, pp 781-789.

[8] A. Amadio, 2006, “Drive-Gas Tailoring For Test-Time Extension Using Unconventional Driver Mixtures”, Masters Thesis, University of Central Florida.

[9] P. Dagaut, J.C. Boettner, and M. Cathonnet, 1996, “Chemical Kinetic Study of Dimethylether Oxidation in a Jet Stirred Reactor from 1 to 10 Atm: Experiments and Kinetic Modeling”, Twenty-Sixth Symposium (International) on Combustion, The Combustion Institute, pp 627-632.

[10] H.J. Curran, W.J. Pitz, C.K. Westbrook, P. Dagaut, J-C Boettner, and M. Cathonnet, 1998, “A Wide Range Modeling Study of Dimethyl Ether Oxidation”, Int. J. Chem. Kinet., **30**, pp 229-241.

[11] T. Amano and F.L. Dryer, 1998, “Effect of Dimethyl Ether, NOx, and Ethane on CH_4 Oxidation: High Pressure, Intermediate-Temperature Experiments and Modeling”, Twenty-Seventh Symposium (International) on Combustion, The Combustion Institute, pp 397-404.

[12] GRI Mech, http://www.me.berkeley.edu/gri-mech/

[13] P. Dagaut, C. Daly, J.M. Simmie, and M. Cathonnet, 1998, “The Oxidation and Ignition of Dimethylether from Low to High Temperature (500-1600 K): Experiments and Kinetic Modeling”, Twenty-Seventh Symposium (International) on Combustion, The Combustion Institute, pp 361-369.

[14] C.A. Frye, A.L. Boehman, and P.J.A. Tijm, 1999, “Comparison of CO and NO Emissions from Propane, n-Butane, and Dimethyl Ether Premixed Flames”, Energy and Fuels, **13**, pp 650-654.

[15] S.L. Fischer, F.L. Dryer, and H.J. Curran, 2000,"The Reaction Kinetics of Dimethyl Ether. I: High-Temperature Pyrolysis and Oxidation in Flow Reactors", Int. J. Chem. Kinet., **32**, pp 713-740.

[16] H.J. Curran, S.L. Fischer, and F.L. Dryer, 2000, "The Reaction Kinetics of Dimethyl Ether. II: Low-Temperature Oxidation in Flow Reactors", Int. J. Chem. Kinet., **32**, pp 741-759.

[17] E.W. Kaiser, T.J. Wallington, M.D. Hurley, J. Platz, H. J Curran, W. J. Pitz, C.K. Westbrook, 2000, "Experimental and Modeling Study of Premixed Atmospheric-Pressure Dimethyl Ether-Air Flames", J. Phys. Chem., **104**, pp 8194-8206.

[18] Y. Hidaka, K. Sato, M. Yamane, 2001, "High-Temperature Pyrolysis of Dimethyl Ether in Shock Waves", Combustion and Flame, **123**, pp 1-22.

[19] F. Maroteaux, G. Descombes, F. Sauton, 2001, "Performance and Exhaust Emissions of A Diesel Engine Running With DME", ICE Spring Technical Conference, **36-1**, pp 73-81.

[20] X. Qin, Y. Ju, and C.K. Law, 2004, "Measurement of Burning Velocities of Dimethyl Ether and Air Premixed Flames at Elevated Pressures", 40th AIAA/ASME/SAE/ASEE Joint Propulsion Conference and Exhibit, July 11-14, Fort Lauderdale, Florida.

[21] X.L. Zheng, T.F. Lu, C.K. Law, C.K. Westbrook, H.J. Curran, 2005, "Experimental and Computational Study of Nonpremixed Ignition of Dimethyl Ether in Counterflow", Proceedings of the Combustion Institute, **30**, pp 1101-1109.

[22] H.J. Curran, 2003, Unpublished Proceedings of the European Combustion Meeting. http://www-cms.llnl.gov/combustion/combustion_home.html

[23] T.A. Semelsberger, R.L. Borup, and H.L. Greene, 2006, "Dimethyl Ether (DME) as an Alternative Fuel", Journal of Power Sources, **156**, pp 497-511.

[24] G.R. Jones, H. Holm-Larson, D. Romani, and R.A. Sills, 2001, "DME for Power Generation Fuel: Supplying India's Southern Region", PetroTech Conference, New Delhi, India.

[25] T. Fleisch and R. Sills, 2004, "Beyond GTL-FT: Large-Scale Gas Conversion Through Oxygenates", 7th Natural Gas Conversion Symposium, Dilian, China.

[26] C.M. Rosado-Reys, J.S. Francisco, J.J. Szente, M.M. Maricq, and L.F. Ostergaard, 2005, "Dimethyl Ether Oxidation at Elevated Temperatures (295-600 K)", J. Phys. Chem., **109**, pp 10940-10953.

[27] C.T. Bowman, D.M. Golden, R.K. Hanson, H. Pitsch, D.F. Davidson, A. Bardos, R. Cook, Z. Hong, S. Jampani, G. Pang, Shashank, K. Walters, L. Wang, R. Malhotra, A. Boehman, and S. Kirby, 2007, "Optimization of Synthetic Oxygenated Fuels for Diesel Engines", GCEP Technical Report. http://gcep.stanford.edu/research/technical_report/2007techreport2.html

[28] H. Seiser, H. Pitsch, K. Seshadri, W.J. Pitz, and H.J. Curran, 2000, "Extinction and Autoignition of N-Heptane in Counterflow Configuration", Proc. Combust. Inst., **28**, pp 2029-2037.

[29] K. Suzaki, k. Tsuchiya, M. Koshi, and A. Tezaki, 2007, "Analysis of HO_2 and OH Formation Mechanisms Using FM and UV Spectroscopy in Dimethyl Ether Oxidation", J. Phys. Chem., **111**, pp 3776-3788.

[30] Z. Chen, X. Qin, Y. Ju, Z. Zhao, M. Chaos, and F.L. Dryer, 2007, "High Temperature Ignition and Combustion Enhancement by Dimethyl Ether Addition to Methane-Air Mixtures", Proceedings of the Combustion Institute, **31**, pp 1215-1222.

[31] Z. Zhao, M. Chaos, A. Kazakov, and F.L. Dryer, 2007, "Thermal Decomposition Reaction and a Comprehensive Kinetic Model of Dimethyl Ether", International Journal of Chemical Kinetics, **40**, pp 1-18.

[32] T.A. Cool, J. Wang, N. Hansen, P.R. Westmoreland, F.L. Dryer, Z. Zhao, A. Kazakov, T. Kasper, and K. Kohse-Hoinghaus, 2007, "Photoionization Mass Spectrometry and Modeling Studies of the Chemistry of Fuel-Rich Dimethyl Ether Flames", Proceedings of the Combustion Institute, **31**, pp 285-193.

[33] A.G. Gaydon and I.R. Hurle, 1963, "The Shock Tube in High-Temperature Chemical Physics", Reinhold Publishing Corporation, NY.

[34] C.T. Bowman and R.K. Hanson, 1979, "Shock tube measurements of rate coefficients of elementary gas reactions," J. Phys. Chem., **83**, pp 757-763.

[35] K.A. Bhaskaran and P. Roth, 2002, "The shock tube as wave reactor for kinetic studies and material systems," Prog. Energy Combust. Sci., **28**, pp 151-192.

[36] I.I. Glass and J.P. Sislian, 2002, "Non Stationary Flows and Shock Waves," (Oxford: Clarenodon).

[37] E.L. Petersen, M.J.A. Richard, M.W. Crofton, E.D. Abbey, M.J. Traum, and D. Kalitan, 2005, "A Facility for Gas- and Condensed-Phase Measurements Behind Shock Waves," Meas. Sci. Technol., **16**, pp 1716-1729.

[38] C.J. Aul, J. deVries, and E.L. Petersen, 2007, "New Shock-Tube Facility for Studies in Chemical Kinetics at Engine Conditions," Eastern States Fall Technical Meeting of the Combustion Institute, Oct. 21-24, Charlottesville, VA.

[39] V. Antonovski, C. Zinner, A. Barrett, D. Kalitan, E. Petersen, D. Healy, H. Curran, and J. Simmie, 2007, "Ignition of Methane/Ethane/Propane Mixtures at Engine Pressure", 5th US Combustion Meeting, March 25-27, San Diego, CA.